LIMNOLOGY and OCEANOGRAPHY

ASLO

Limnol. Oceanogr. 65, 2020, 2056–2075

doi: 10.1002/lno.11437

Dynamics of an intense diatom bloom in the Northern Antarctic Peninsula, February 2016

Raul Rodrigo Costa,[1,2*] **Carlos Rafael Borges Mendes**,[1,2] **Virginia Maria Tavano**,[1,2] **Tiago Segabinazzi Dotto**,[2] **Rodrigo Kerr**,[2] **Thiago Monteiro**,[2] **Clarisse Odebrecht**,[1] **Eduardo Resende Secchi**[3]

[1]Laboratório de Fitoplâncton e Microorganismos Marinhos, Instituto de Oceanografia, Universidade Federal do Rio Grande (FURG), Av. Itália, km 8, Rio Grande, RS, Brazil

[2]Laboratório de Estudos dos Oceanos e Clima, Instituto de Oceanografia, Universidade Federal do Rio Grande (FURG), Rio Grande, RS, Brazil

[3]Laboratório de Ecologia e Conservação da Megafauna Marinha, Instituto de Oceanografia, Universidade Federal do Rio Grande (FURG), Rio Grande, RS, Brazil

Abstract

Diatoms are considered the main base of the Southern Ocean food web as they are responsible for more than 85% of its annual primary production and play a crucial role in the Antarctic trophic structure and in the biogeochemical cycles. Within this context, an intense diatom bloom reaching > 45 mg m^{-3} of chlorophyll *a* was registered in the Northern Antarctic Peninsula (NAP) during a late summer study in February 2016. Given that nutrient concentrations and grazing activities were not identified here as limiting factors on the bloom development, the aim of this study was to evaluate the effect of water column structure (stability and upper mixed layer depth) on the phytoplankton biomass and composition in the NAP. The diatom bloom, mainly composed by the large centric *Odontella weissflogii* (mostly > 70 μm in length), was associated with a local ocean carbon dioxide uptake that reached values greater than −60 mmol m^{-2} d^{-1}. We hypothesize that the presence of a vertically large water column stability barrier, just below the pycnocline, was the main driver allowing for the development of the intense diatom bloom, particularly in the Gerlache Strait. Contrarily, a shift from diatoms to dinoflagellates (mainly Gymnodiniales < 20 μm) was observed associated with conditions of a highly stable thin layer. The results suggest that a large fraction of this intense diatom bloom is in fast sinking process, associated with low grazing pressure, showing a crucial role of diatoms for the efficiency of the biological carbon pump in this region.

The Antarctic Peninsula has experienced one of the largest warming rates on Earth during the last 50 years (Ducklow et al. 2007), including a significant warming of the oceanic surface waters (Meredith and King 2005; Couto et al. 2017). In addition, the warming of the atmosphere has been linked to sea ice dynamics, affecting the timing of the sea ice formation and melting (Smith and Stammerjohn 2001; Stammerjohn et al. 2008; Turner et al. 2013). As life histories of most Antarctic organisms are attuned to sea ice, the recent atmospheric warming of the Antarctic Peninsula and consequent changes in the seasonality of the sea ice cover (e.g., Turner et al. 2015; Massom et al. 2018) have been associated with changes in key food web trophic levels. This includes shifts in the composition of phytoplankton community and decrease in the abundance of Antarctic krill, with direct consequences throughout the whole regional ecosystem (Moline et al. 2004; Ducklow et al. 2007; Montes-Hugo et al. 2009; Seyboth et al. 2018).

Diatoms, a dominant phytoplankton group in the Southern Ocean (e.g., Arrigo et al. 1999; Pondaven et al. 2000; Armbrust 2009), are considered the core of the austral food web as they are responsible for more than 85% of its annual primary production (Rousseaux and Gregg 2014). Consequently, the diatoms play crucial role in the trophic structure and biogeochemical cycles of the region (Falkowski et al. 1998; Tréguer et al. 2017; Person et al. 2018; Brown et al. 2019). Although this group seems well adapted to regimes of intermittent light and nutrient exposure, it is particularly common in nutrient-rich environments encompassing polar regions, as

*Correspondence: costa@furg.br

Additional Supporting Information may be found in the online version of this article.

well as upwelling and coastal areas (Smetacek et al. 2012). Such characteristics highlight its success in occupying a wide range of ecological niches and biomes (Malviya et al. 2016). However, despite their importance for the Antarctic ecosystems and in the marine carbon cycle, the current knowledge on ecology and distribution of diatoms in the Southern Ocean remains generalized at best.

The Northern Antarctic Peninsula (NAP), which encompasses the Gerlache and Bransfield Straits, the southernmost sector of the Drake Passage, the northwestern Weddell Sea and the regions offshore of the western Antarctic Peninsula, is a good example of how environmental changes can alter and transform the polar ecosystem through time (Kerr et al. 2018*c* and references therein). This is a highly productive area and a key-feeding region for whales (e.g., Dalla Rosa et al. 2008; Nowacek et al. 2011; Secchi et al. 2011; Seyboth et al. 2018) and other krill-feeding predators (e.g., Trivelpiece et al. 2011; Southwell et al. 2012). The relevance of the NAP as a foraging ground is probably related to the high local biological productivity (Rodriguez et al. 2002; Varela et al. 2002), usually dominated by diatoms, but can also be positively impacted by or benefited from the physical complexity of hydrography and circulation, sea ice dynamics, continental meltwater input, and protection from severe weather (Prézelin et al. 2000, 2004).

The high phytoplankton productivity in the Antarctic waters, particularly in coastal regions, is fuelled by an abundant supply of nutrients and the availability of light when the mixed layers are shallow, thus allowing cells to overcome light limitation (Mendes et al. 2012; Rozema et al. 2017; Schofield et al. 2017). Recent studies have shown that the NAP is also being affected by several environmental factors, such as early retreat of sea ice and increase in sea surface temperature, which have been associated with an increase in occurrence and abundance of certain phytoplankton groups, such as cryptophytes (Moline et al. 2004; Montes-Hugo et al. 2009; Mendes et al. 2013, 2018*a*,*b*). As diatoms are more efficiently grazed by Antarctic krill than cryptophytes (Haberman et al. 2003), the shift from a diatoms- to a cryptophyte-dominated community may affect food web trophic interactions and, consequently, the ecology of the local marine food web (Moline et al. 2004; Ducklow et al. 2007). Due to intensification of meltwater conditions in the Southern Ocean, the water column stability has been pointed as an important driver controlling the biomass and composition of phytoplankton communities (Dierssen et al. 2002; Moline et al. 2004; Mendes et al. 2012; Höfer et al. 2019). Therefore, studies on phytoplankton and the influence of environmental constraints in species/groups composition are relevant to evaluate ecosystem changes on short- and long-term scales.

Although the ecological and biogeochemical relevance of diatom blooms to the Antarctic ecosystem are well known (e.g., Rodriguez et al. 2002; Varela et al. 2002; Garibotti et al. 2005), in situ measurements of the prevailing environmental conditions during the period of development and establishment of the blooms are scarce and almost unexplored. In this context, we reported here in loco observations of an intense diatom bloom dominated by the large (mostly > 70 μm in length) centric diatom *Odontella weissflogii*, spanning a vast area of the NAP during a late summer oceanographic survey conducted in February 2016, and described its biogeochemical role in that environment. Results presented here contribute to a better understanding of the causal linkages between environmental conditions and the composition of the phytoplankton community during diatom blooms in the Antarctic Peninsula. Moreover, this study elucidates factors that can disrupt ecosystem balance in a critically important Antarctic coastal region.

Material and methods

Cruise design and sampling collection

The data set was collected during an oceanographic cruise conducted on board the *RV Almirante Maximiano* of the Brazilian Navy along of the NAP, during late summer of 2016 (from 14 to 24 February; 40 stations). The study area covered the Gerlache Strait, which separates the Anvers and Brabant Islands from the Antarctic Peninsula, the Bransfield Strait, between the southern Shetland Islands and the Peninsula, and the north-eastern Bellingshausen Sea (Fig. 1). Therefore, in order to better evaluate the effects of hydrographic properties on the phytoplankton community, the sampling stations were split into three data sets (different symbols in Fig. 1): the region under higher influence of waters advected from the Bellinghausen Sea (Bellingshausen), the Gerlache Strait (Gerlache), and the Bransfield Strait region (Bransfield).

Hydrographic data profiles (temperature and salinity) and seawater discrete samples were collected using a combined Sea-Bird CTD/Carrousel 911 + system® equipped with 24, 5-L Niskin bottles. Surface seawater samples were taken in all conductivity–temperature–depth stations for both dissolved nutrients and phytoplankton pigments analyses. At some stations, chosen based on the downcast fluorescence profiles (WetLabs® profiling fluorometer), seawater samples were taken from several depths between the surface and 150 m to characterize the vertical distribution of phytoplankton communities. However, due to the absence of deep chlorophyll maximum (DCM) layers, seawater samples at these selected stations were generally collected at regular depths of 5 (hereafter defined as surface), 25, 50, 75, 100, and 150 m. In order to investigate differences in phytoplankton composition between regions, five surface sampling stations were selected for microscopic analysis, that is, Stas. G10 and G13, in Gerlache Strait; Stas. I18 and I16, in north-eastern Bellingshausen Sea; and Sta. B33 in Bransfield Strait (Fig. 1).

Additionally, to complement the phytoplankton taxonomic information, size fractionation of phytoplankton chlorophyll *a* (Chl *a*) biomass was performed at 10 selected surface samples, which were representative of the study region. The fractionation was carried out by sequential filtering of water

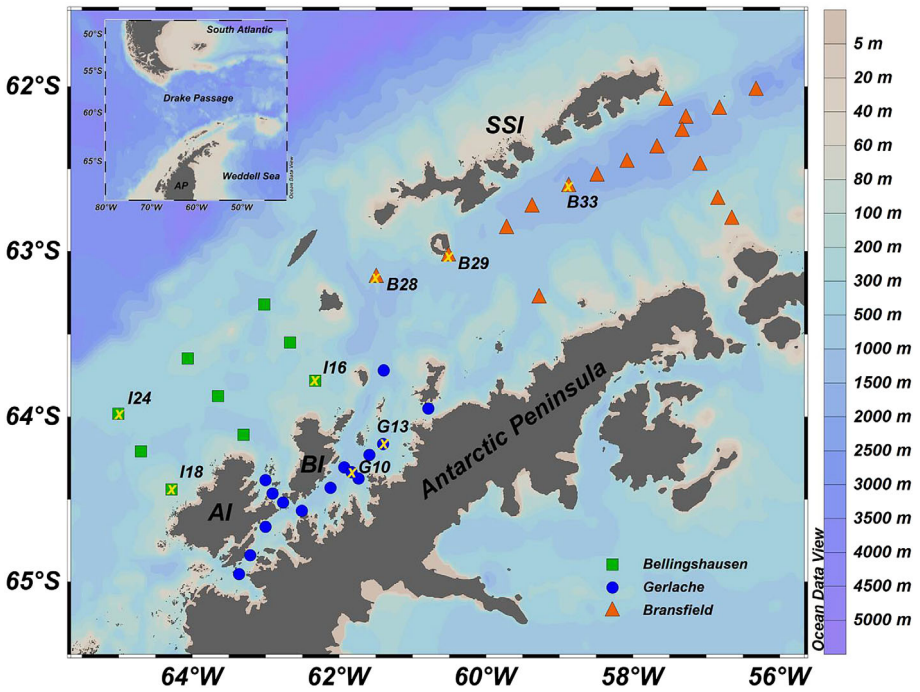

Fig. 1. Study area and stations' locations during 2016 in the late austral summer cruise. Hydrographic stations positions are marked by circles, squares, and triangles, indicating zones characterized by Gerlache, Bellingshausen, and Bransfield surface waters, respectively. Labeled stations with "x" indicate locations where high-resolution vertical pigments' profiles are available. The bathymetry is represented by the color scale bar on the right. An inset map in the upper left corner shows a larger area that pinpoints where the main map is located. The abbreviations are as follows: AI, Anvers Island; AP, Antarctic Peninsula; BI, Brabant Island; SSI, South Shetland Islands.

subsamples (1000 mL). Each sample was firstly filtered using a polycarbonate filter with pore size of 20 μm (GE Water & Process Technologies, 47 mm). The collected filtrate was subsequently filtered into a polycarbonate filter with pore size of 2 μm (GE Water & Process Technologies, 47 mm). Lastly, the collected filtrate was filtered into GF/F filter (Whatman) to retain the cells between 0.7 and 2 μm. The first two filtrations were performed by gravity and the last one under low vacuum pump (< 5 in. Hg). The filtration by gravity minimizes the problems of vacuum filtration, such as breaking phytoplankton cells. This procedure yielded high-performance liquid chromatography (HPLC) measured Chl *a* concentration for the picophytoplankton (between 0.7 and 2 μm), nanophytoplankton (2–20 μm), and microphytoplankton (> 20 μm).

Physical measurements

The seawater potential density (ρ, kg m^{-3}) was determined based on seawater potential temperature, salinity, and pressure data in order to evaluate the physical structure of the water column. The upper mixed layer depth (UMLD) was determined as the depth at which ρ deviate from its 10 m depth value by a threshold of $\Delta\rho$ = 0.03 kg m^{-3} (de Boyer Montégut et al. 2004). The water column stability was estimated using vertical ρ variations, as a function of buoyancy or the Brunt–Väisälä frequency (N^2), which is determined by

$$N^2 = -\frac{g}{\rho}\frac{\partial \rho}{\partial z}\left(\mathrm{rad^2 s^{-2}}\right),$$

where g is gravity, z is the water depth, and ρ is the potential density of seawater. The water column stability (E) was further estimated from

$$E = \frac{N^2}{g}\left(10^{-6}\,\mathrm{rad^2 m^{-1}}\right).$$

In order to represent the horizontal variation of stability within the upper layers of water column along the three regions, we tried three different forms of stability values: mean stability between 0 and 150 m (depth range where biological samples were taken), mean stability within the upper mixed layer, and peak stability value directly below the UMLD. Since a good linear correlation was found between the three forms (data not shown), the mean stability between 0 and 150 m (hereafter referred to as stability and represented by the parameter E) was then selected to be used in this study to show the horizontal variation of water column stability values, to keep the same approach as in previous works of the group (e.g., Mendes et al. 2012, 2013, 2018*a*,*b*).

To evaluate the effects of freshwater input on the structure of phytoplankton communities, the meltwater percentage (%MW) was estimated, following Rivaro et al. (2014), as:

$$\%\mathrm{MW} = \left(1 - \frac{S_{\mathrm{meas}} - 6}{S_{\mathrm{deep}} - 6}\right) \times 100.$$

The equation above considers the ratio of the difference between the measured surface seawater salinity (S_{meas}) and at a greater depth (S_{deep}; i.e., at 300 m), which was presumably not influenced by freshwater from sea ice dilution and continental melting on the same station, and the average sea ice salinity of 6 (Ackley et al. 1979).

The euphotic layer depth (Z_{eu}) is defined as the depth where the downwelling photosynthetically available radiation (λ = 400–700 nm) is reduced to 1% of its value at surface. A direct measure of Z_{eu} was not available in the present study. Therefore, Z_{eu} was estimated as:

$$\log_{10}(z_{\mathrm{eu}}) = -0.45 \times \log_{10}(\mathrm{Chl}\,a) + 1.79,$$

where the surface Chl *a* concentration was used. This equation was developed by an empirical relationship derived from measured Z_{eu} and Chl *a* concentration, measured at 5 m for daylight stations and obtained during two oceanographic surveys conducted in the same region covered in this study (Ferreira et al. 2017).

Dissolved nutrients analysis

Surface seawater samples were filtered through cellulose acetate membrane filters to determine dissolved inorganic nutrients (i.e., dissolved inorganic nitrogen [DIN]: nitrate, nitrite, and ammonium; phosphate and silicic acid). The samples were immediately frozen at −20°C until the laboratory analysis. Nutrients were analyzed at the Laboratory of Biogeochemistry at the Federal University of Rio de Janeiro, Brazil, following the spectrophotometric determination methods described by Aminot and Chaussepied (1983). Orthophosphate was measured by reaction with ammonium molybdate, with absorption readings at 885 nm. Silicic acid measurements, in the form of reactive Si, were corrected for sea salt interference.

HPLC pigment analysis

For phytoplankton pigment analysis, seawater samples (0.5–2.5 L) were filtered under low vacuum through GF/F filters and these were immediately frozen in liquid nitrogen for later HPLC pigment analysis. In the laboratory, the filters were placed in a screw cap centrifuge tube with 3 mL of 95% cold-buffered methanol (2% ammonium acetate) containing 0.05 mg L^{-1} trans-β-apo-8′-carotenal (Fluka) as internal standard. Samples were sonicated for 5 min in an ice-water bath, placed at −20°C for 1 h, and then centrifuged at 1100 g for 5 min at 3°C. The supernatants were filtered through Fluoropore PTFE membrane filters (0.2 μm pore size) to separate the extract from remains of filter and cell debris. Immediately prior to injection, 1000 μL of sample was mixed with 400 μL of Milli-Q water in 2.0-mL amber glass sample vials, which then were placed in the HPLC cooling rack (4°C). The pigment extracts were analyzed using a Shimadzu HPLC constituted by a solvent distributor module (LC-20 AD) with a control system (CBM-20A), a photodiode detector (SPDM20A), and a fluorescence detector (RF-10AXL). The chromatographic separation of the pigments was performed using a monomeric C8 column (SunFire; 15 cm long; 4.6 mm in diameter; 3.5 μm particle size) at a constant temperature of 25°C. The mobile phase (solvent) and respective gradient followed the method developed by Zapata et al. (2000), discussed and optimized by Mendes et al. (2007), with a flow rate of 1 mL min^{-1}, injection volume of 100 μL, and 40 min runs. All the studied pigments were identified from both absorbance spectra and retention times, and the concentrations were calculated from the signals in the photodiode array detector in comparison with commercial standards obtained from DHI (Institute for Water and Environment, Denmark). The peaks were integrated using LC-Solution software, and all of the peak integrations were checked manually and corrected when necessary. A quality assurance threshold procedure, through application of limit of quantification (LOQ) and limit of detection (LOD), was applied to the pigment data as described by Hooker et al. (2005) to reduce the uncertainty of pigments found in low concentrations. The LOQ and LOD procedures were performed according to Mendes et al. (2007). In order to correct for losses and volume changes, the concentrations of the pigments were normalized to the internal standard.

The HPLC analysis allowed separation, identification, and quantification of three types of Chl *a* degradation products: chlorophyllide *a* (Chlide *a*), pheophytin *a* (Phytin *a*), and pheophorbide *a* (Pheide *a*). The relative content of those degradation products can be used as a proxy for grazing pressure and for senescence of phytoplankton cells (e.g., Jeffrey 1974; Mendes et al. 2012; Pillai et al. 2018). Thus, the sum of the Phytin *a* and Phide *a* was used as a proxy of zooplankton assemblage grazing, while Chlide *a* was used as senescence index of the phytoplankton community.

Chemical taxonomy analysis of pigment data

The relative contribution of phytoplankton groups to the overall biomass was calculated from the class-specific accessory pigments and total Chl *a* using the Chemical taxonomy (CHEMTAX) software v1.95 (Mackey et al. 1996). CHEMTAX uses a factor analysis and steepest descent algorithm to best fit the data onto an initial matrix of pigment ratios (the ratios between the respective accessory pigments and Chl *a*). This software package has been extensively and successfully used in many worldwide investigations (Mendes et al. 2011; Schlüter et al. 2011; Araujo et al. 2017; Carvalho et al. 2019; Lima et al. 2019), including in the Southern Ocean (e.g., Rodríguez et al. 2002; Wright et al. 2010; Mendes et al. 2012, 2015), to determine the distribution and Chl *a* biomass

of phytoplankton functional groups. This approach provides valuable information about the whole phytoplankton community, including small-size species, which are normally difficult to identify by light microscopy. The basis for calculations and procedures is fully described by Mendes et al. (2018*a*). Although concentration of Chl *a* is not an absolute measure of algal biomass, such as carbon, it can be used as a proxy for biomass (Jeffrey et al. 1997; Huot et al. 2007), since this photosynthetic pigment is common to all autotrophic phytoplankton. Therefore, in this work, we use the term Chl *a* referring to either total biomass or relative biomass attributed to the corresponding taxonomic groups, as has been widely applied with the CHEMTAX approach.

Six algal groups were chosen for CHEMTAX analysis based on previous experience in the region (Mendes et al. 2012, 2013, 2018*a*,*b*) and confirmation of the higher taxonomic groups by microscopy. The algal groups chosen are diatoms, dinoflagellates-A (peridinin-containing dinoflagellates), dinoflagellates-B (containing gyroxanthin esters and fucoxanthin derivatives), "*Phaeocystis antarctica*," cryptophytes and green flagellates. Although Mendes et al. (2018*a*) have used a 7-class CHEMTAX approach, including two types of diatoms—Type A (containing typical diatom pigmentation; Chl c_1, Chl c_2, fucoxanthin, and diadinoxanthin) and Type B, where Chl c_3 replaces Chl c_1—in this work, we chose to use only one group of diatoms due to absence of Chl c_1 in the samples analyzed. In addition, the strong correlation between Chl c_3 and fucoxanthin, in association with the large abundances/biomasses of diatoms, allowed us to assert that the assemblage of diatoms occurring in the study area (mainly *O. weissflogii*) was Type B.

The whole pigment data set was separated in three distinct oceanographic provinces addressed in this study: Bransfield, Gerlache, and Bellinghausen. In order to account for pigment ratios' variations with irradiance, these three data sets were further split into three bins according to sample depth (0–25, 25–50, and > 50 m), each of which was separately analyzed by CHEMTAX to allow for variation in pigment: Chl *a* ratios with depth (Mackey et al. 1998). This procedure assured homogeneity of the pigment: Chl *a* ratios within all samples from the same bin, providing some compensation for changes in these ratios, which are known to vary with light availability (Schlüter et al. 2000; Higgins et al. 2011). Regarding the fractionation data, the split of pigment data set was performed according to size class (> 20, 2–20, and 0.7–2 μm). For optimization of the input matrix, a series of 60 pigment ratio matrices were generated by multiplying each ratio from the initial matrix by a random function as described by Wright et al. (2009). The averages of the best six (10%) output matrices, with the lowest residual or mean square root error, were taken as the optimized results. The initial and optimized pigment ratio matrices derived from CHEMTAX are presented in Supporting Information Tables S1 and S2.

Microscopic analysis

The samples collected at surface were preserved in amber glass flasks (± 250 mL) with 2% alkaline Lugol's iodine solution in order to evaluate the species composition and cell density of the phytoplankton assemblage. Settling chambers (2, 10, or 50 mL settling volume) were inspected on an Axiovert 135 ZEISS inverted microscopic (Utermöhl 1958; Sournia 1978) at 100×, 200×, and 400× magnification, following previous literature (e.g., Scott and Marchant 2005). Species-specific cell biovolumes were estimated by measuring cell dimensions (such as length, width, and height) and applying respective similar geometric shapes as in Hillebrand et al. (1999). The most abundant species were selected for the biovolume calculation as represented in Supporting Information Table S3.

CO_2 partial pressure and sea–air fluxes

We estimated the carbon dioxide (CO_2) partial pressure in surface seawater (pCO_2^{sw}) based on the total alkalinity and total dissolved inorganic carbon measurements, using the CO2SYS program v2.1 (Lewis et al. 1998; Pierrot et al. 2006). The pCO_2^{sw} error associated with this indirect calculation was estimated to be at least ±5.7 μatm. We used the carbonate dissociation constants K1 and K2 proposed by Goeyt and Poisson (1989) and the sulfate and borate constants proposed by Dickson (1990) and Uppström (1974), respectively. Those constants have a good response and are recommended for high latitude regions (e.g., Laika et al. 2009; Kerr et al. 2018*a*). Total alkalinity and total dissolved inorganic carbon were determined simultaneously by potentiometric titration in a closed cell (Dickson et al. 2007). To ensure the best performance from these analyses, we used certified reference material batch no. 149 (Dickson et al. 2003). The analytical precision of total alkalinity and total dissolved inorganic carbon measurements were investigated daily through replicate analyses of a single sample and was determined to be ±4.4 and ± 2.7 μmol kg^{-1}, respectively.

The net sea–air CO_2 flux (FCO_2) was calculated by the following equation:

$$FCO_2 = K_t K_s \Delta pCO_2,$$

where ΔpCO_2 is the difference between pCO_2^{sw} and CO_2 partial pressure in the atmosphere (pCO_2^{air}); K_t is the gas transfer velocity as a function of wind speed, which we calculated using the latest K_t relationship (Wanninkhof 2014); and K_s is the CO_2 solubility coefficient, which was calculated as a function of both temperature and salinity (Weiss 1974). Both the pCO_2^{air} and wind speed used here were determined from measurements obtained at the U.S. Palmer Station (Dlugokencky et al. 2015). We used the monthly pCO_2^{air} average (397.9 ± 0.48 μatm) for February 2016 to calculate the

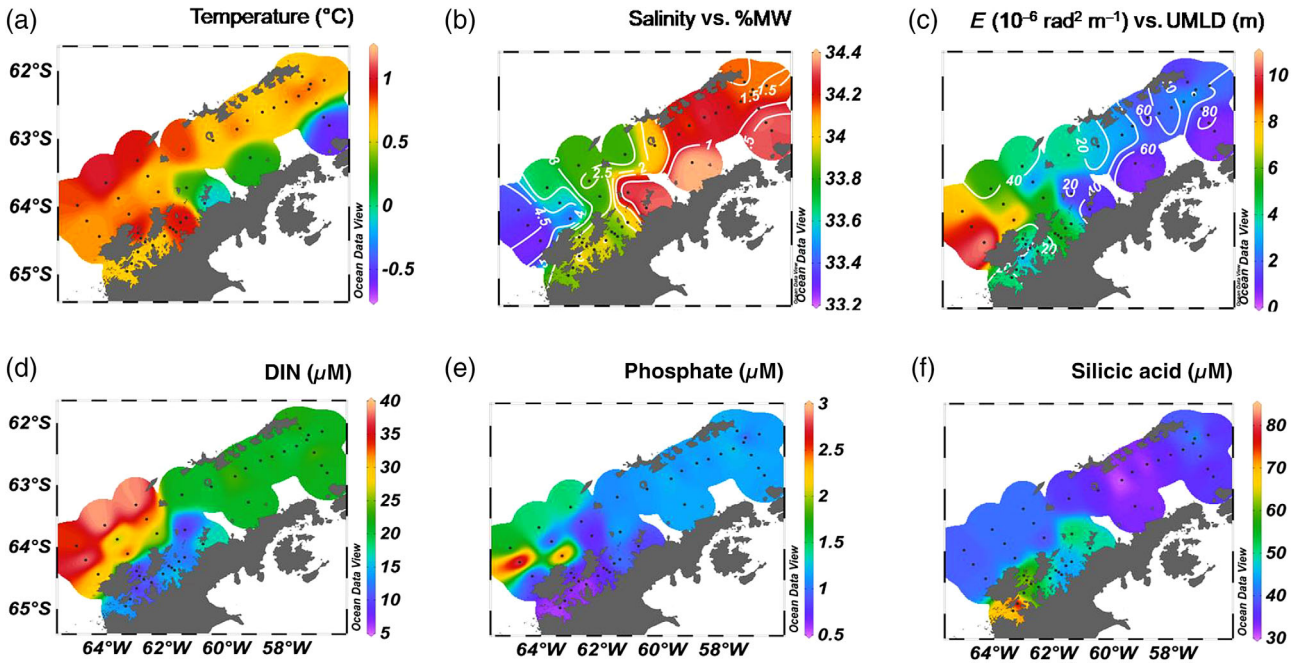

Fig. 2. Surface distributions of temperature (**a**), both salinity (color scale) and %MW (contour lines) (**b**), both mean stability (*E*; color scale) and UMLD (contour lines) (**c**), DIN (**d**), phosphate (**e**), and silicic acid (**f**). Black dots represent stations' location.

ΔpCO_2 across all sampling stations. For the calculation of FCO_2, we used weekly averages of wind speed to ensure that the whole effect of wind action is acting on CO_2 exchanges at the sea–air surface boundary.

Statistical analysis

Relationships between Chl *a* biomass of phytoplankton groups and environmental variables at surface (except for determining water column structure, where data from the upper 150 m were used) were estimated through canonical correspondence analysis (CCA; Ter Braak and Prentice 1988) using CANOCO for Windows 4.5 software. This analysis was performed in order to identify the main patterns of the phytoplankton community structure with respect to environmental variables. Biotic variables were represented by the CHEMTAX-derived taxonomical groups' biomass (mg m^{-3} of Chl *a*). Environmental variables included stability (mean between 0 and 150 m), UMLD, %MW, sea surface temperature (T), sea surface salinity (Salinity), DIN, phosphate, and silicic acid. All variables were log transformed before analysis to reduce the influence of different scales in the data sets. Monte Carlo tests were run based on 499 permutations under a reduced model ($p < 0.01$) in order to evaluate the significance of the CCA.

Results

Environmental setting

The surface environmental properties showed a well-defined gradient along the NAP (Fig. 2), reflecting marked

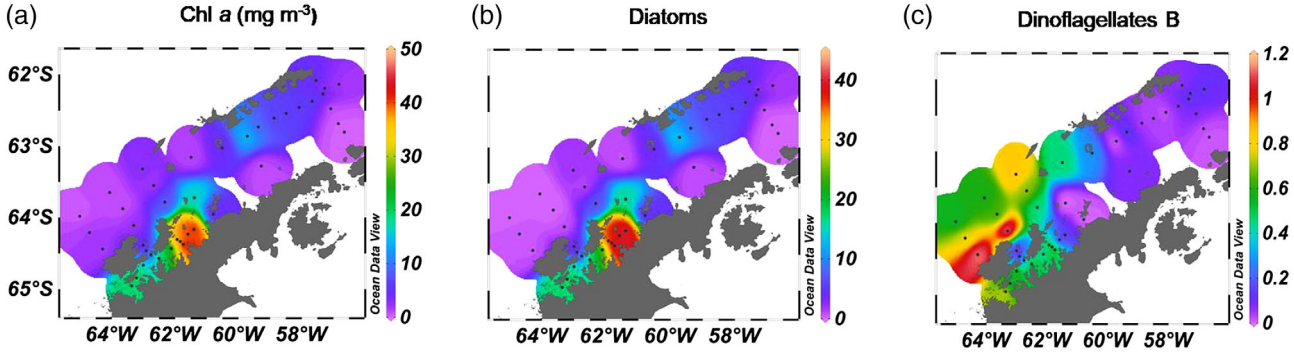

Fig. 3. Surface distribution of total Chl *a* (mg m^{-3}) (**a**), absolute contribution of diatoms to total Chl *a* (mg m^{-3}) (**b**), absolute contribution of dinoflagellates Type B to total Chl *a* (mg m^{-3}) (**c**). Note the different scales. Black dots represent stations' location.

oceanographic contrast between the subregions under investigation (i.e., Bellingshausen, Bransfield, and Gerlache). The temperature distribution shows the influence of waters from Bellingshausen Sea (i.e., warm) and Weddell Sea (i.e., cold) along the Antarctic Peninsula (Fig. 2a), including the presence of the Peninsula Front (Sangrà et al. 2011). The influence of a freshwater layer is clearly seen on the Bellingshausen zone associated with the minima salinity values of the study area (Fig. 2b).

A gradual decrease in mean stability was registered in the upper water layers (0–150 m) from Bellingshausen towards the Gerlache and Bransfield straits (Fig. 2c). The highest averaged stability value of 6.71×10^{-6} rad^2 m^{-1} is seen in Bellingshausen and the lowest stability value of 2.08×10^{-6} rad^2 m^{-1} is observed in Bransfield. The sea surface temperature distribution (Fig. 2a) has an opposite pattern with sea surface salinity (Fig. 2b). The Bellingshausen showed the highest mean sea surface temperature value of 0.81°C associated with lowest mean sea surface

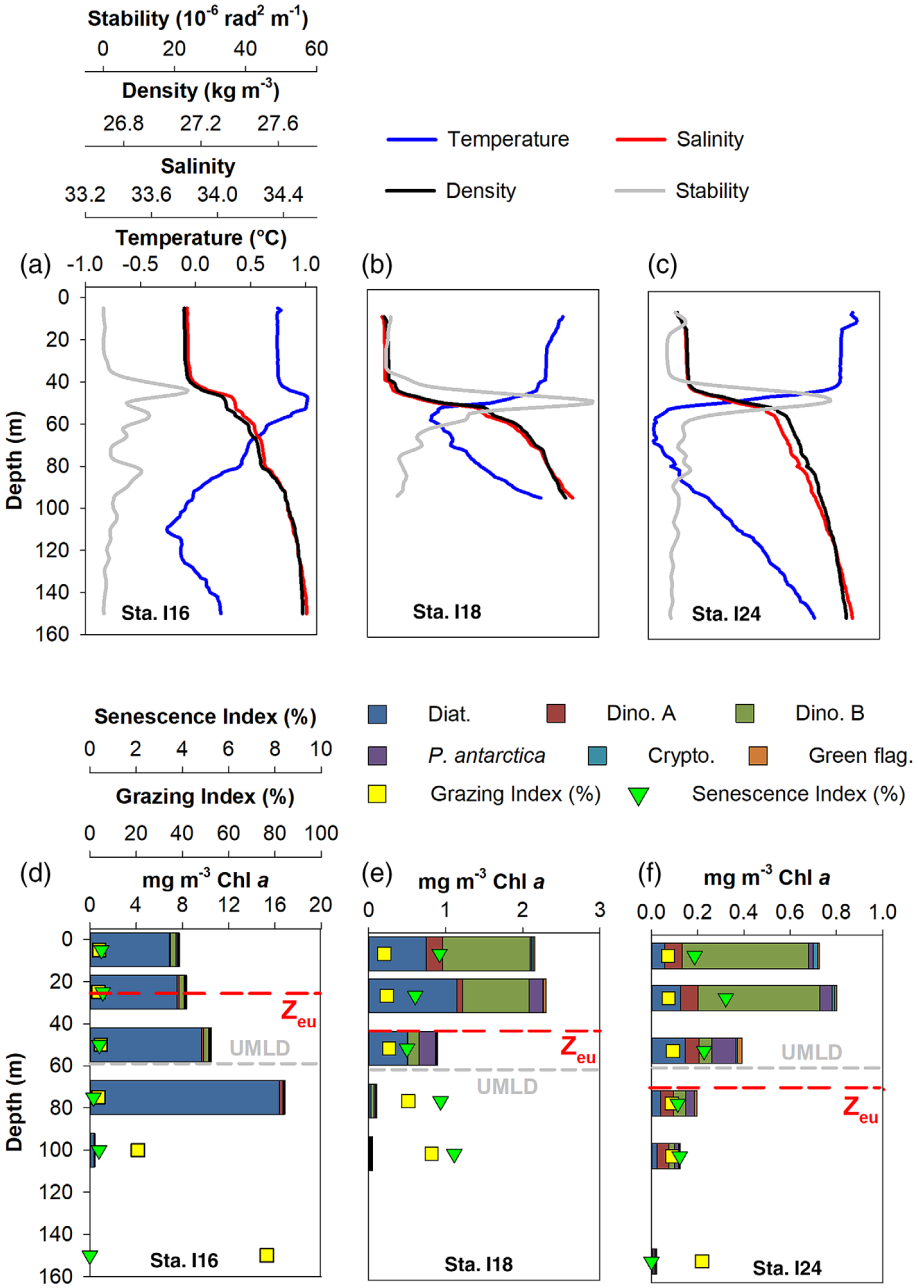

Fig. 4. Vertical profiles of water column salinity, temperature, density and stability (top panel) to stations: Sta. I16 (**a**), Sta. I18 (**b**), and Sta. I24 (**c**), in Bellingshausen region, and depth distribution of phytoplankton groups' biomass (as chlorophyll *a* concentration) calculated by CHEMTAX to same stations: Sta. I16 (**d**), Sta. I18 (**e**), and Sta. I24 (**f**), along with their respective UMLD (gray horizontal dashed lines) and euphotic zone (Z_{eu}; red horizontal dashed lines), as well as both grazing (yellow squares) and senescence (green triangles) indices, represented in the lower panel.

salinity of 33.57, Gerlache showed mean intermediate values of both temperature (0.70°C) and salinity (33.98), whereas Bransfield showed the lowest mean temperature of 0.54°C associated with the highest mean salinity value of 34.19 (*see* Supporting Information Table S4).

The freshwater input, represented by %MW, showed a noticeable southwest–northeast surface gradient associated with surface salinity values, where the lower (higher) sea surface salinities were recorded in association with the higher (lower) values of % MW (*see* Fig. 2b). The pattern presented by the UMLD, in turn, is not associated with any other variable (Fig. 2c). It shows high averaged values of 47 ± 25 m registered in Bransfield, intermediate values in Bellinghausen (34 ± 9 m), and the lowest UMLD values in the Gerlache Strait (23 ± 9 m). The euphotic zone depth (Z_{eu}) of ~ 45 m was very similar in Bellingshausen and Bransfield zones, whereas on the Gerlache Strait this depth decreases to ~ 20 m (*see* Supporting Information Table S4).

The surface nutrient concentrations were relatively high throughout the study area (Supporting Information Table S4). However, there was a considerable spatial variability, for example, in silicic acid concentrations, whose values were substantially higher in Gerlache Strait. In turn, Gerlache Strait presented the lowest DIN and phosphate values (Fig. 2d–f).

Phytoplankton Chl *a* biomass and community composition

The surface Chl *a* concentration, ranging from 0.3 to 46.5 mg m^{-3}, varied significantly along the NAP (Fig. 3a). Three clear spatial features associated with each subregion were observed: (1) high Chl *a* region greater than 45 mg m^{-3} in the Gerlache Strait; (2) intermediate Chl *a* levels varying between 10 and 15 mg m^{-3} in the deep zones of the Bransfield central basin; and (3) low Chl *a* concentration (< 2 mg m^{-3}) observed in the Bellingshausen region and southeast of the Peninsula Front (i.e., stations influenced by Weddell Sea waters advected into the Bransfield Strait).

Phytoplankton assemblages were generally dominated by diatoms (Fig. 3b), especially at stations with high Chl *a* concentration (Fig. 3a). In the northern Gerlache Strait and at the center of the Bransfield Strait, diatom's contributions were higher than 90% of total Chl *a*. The predominant species in those blooms was the large centric diatom *O. weissflogii* (mostly > 70 μm in length), as identified by microscopic analysis (Supporting Information Table S3). Dinoflagellates Type B (mainly small Gymnodiniales < 20 μm; Table S3) appeared as the second most representative taxonomic group (Fig. 3c), particularly at the Bellingshausen stations with higher %MW and lower salinities (Fig. 2b). Dinoflagellates Type A, cryptophytes, *P. antarctica*, and green flagellates showed much lower Chl *a* biomass, and their contributions were more significant at stations with low values of Chl *a* (Supporting Information Fig. S1).

Due to the presence of the low salinity surface layers, the Bellingshausen region displayed an evident shift between the main phytoplankton groups, as a result of the increased stability immediately below the UMLD (Fig. 4a–c). Lower Chl *a* biomass and an increase in contribution of dinoflagellates-B over diatoms were observed at stations with high stability values

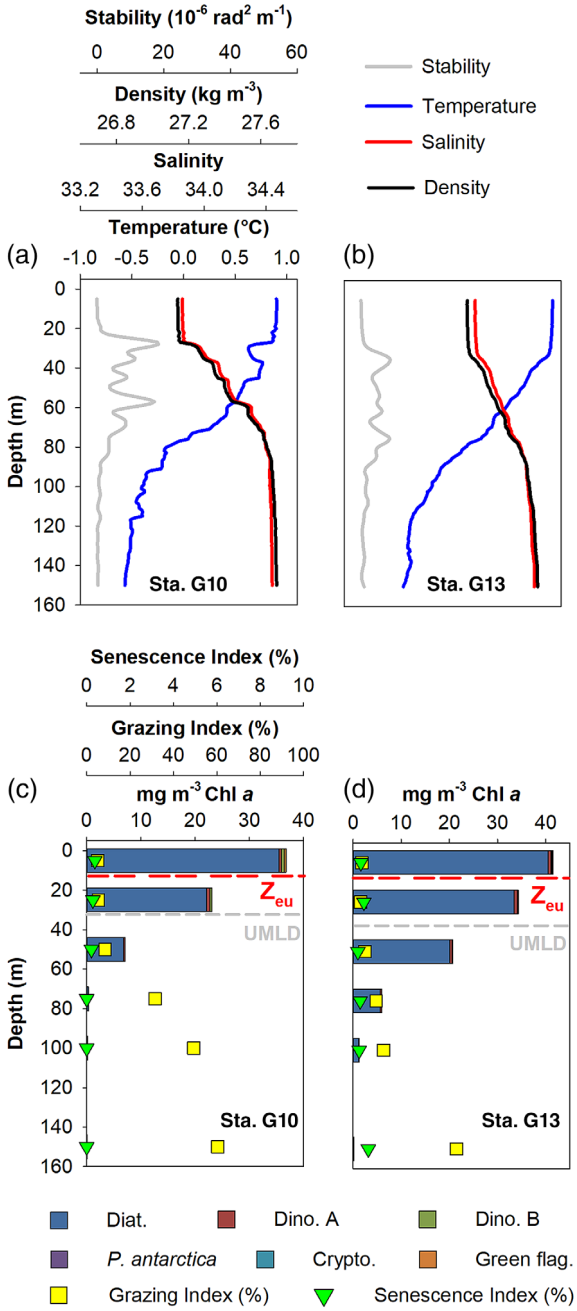

Fig. 5. Vertical profiles of water column salinity, temperature, density, and stability (top panel) to stations: Sta. G10 (**a**) and Sta. G13 (**b**), in Gerlache region, and depth distribution of phytoplankton groups' biomass (as chlorophyll *a* concentration) calculated by CHEMTAX to same stations: Sta. G10 (**c**) and Sta. G13 (**d**), along with their respective UMLD (gray horizontal dashed lines) and euphotic zone (Z_{eu}; red horizontal dashed lines), as well as both grazing (yellow squares) and senescence (green triangles) indices, represented in the lower panel.

(Fig. 4d–f), particularly associated with the formation of a thin layer of high stability that markedly separated the water column above and below the UMLD (*see* Fig. 4b,c). Inversely, the Gerlache and Bransfield Straits were absolutely dominated by diatoms associated with lower variation of the water column stability (*see* Figs. 5, 6, respectively). However, it was possible to observe substantial differences in the intensity (Chl *a* biomass) and in vertical distribution of these blooms between the Gerlache and Bransfield Straits. In Gerlache, the diatom blooms were conspicuously found in shallow upper mixed layers (0–25 m) (Fig. 5c,d). These profiles showed a distinct pattern of stability/density at the pycnocline (Fig. 5a,b), corresponding to a large stable thick layer of ~ 50 m with several stability peaks. In the Bransfield Strait, despite the absolute dominance of diatoms at most stations, lower Chl *a* concentrations were found

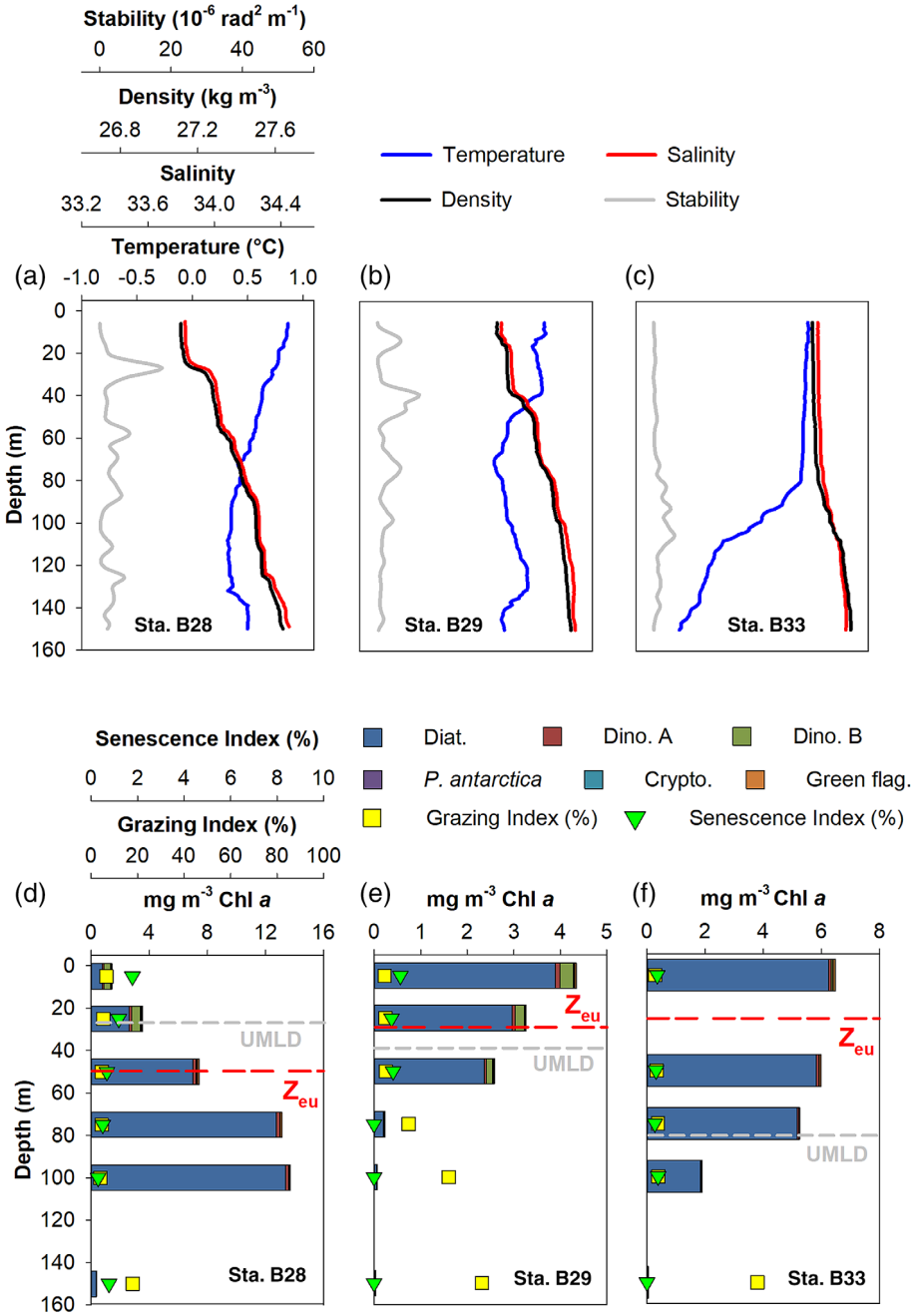

Fig. 6. Vertical profiles of water column salinity, temperature, density, and stability (top panel) at stations: Sta. B28 (**a**), Sta. B29 (**b**), and Sta. B33 (**c**), in Bransfield region, and depth distribution of phytoplankton groups' biomass (as Chl *a* concentration) calculated by CHEMTAX at same stations: Sta. B28 (**d**), Sta. B29 (**e**), and Sta. B33 (**f**), along with their respective UMLD (gray horizontal dashed lines) and euphotic zone (Z_{eu}; red horizontal dashed lines), as well as both grazing (yellow squares) and senescence (green triangles) indices, represented in the lower panel.

(Fig. 6d–f), associated with less stable water columns (Fig. 6a–c).

Grazing and senescence indices

The mean level of degradation products associated with grazing processes was similar in all regions. Generally, it was characterized by low values within the upper mixed layer (with an average proportion frequently below 5%), and increased levels below the UMLD in association with very low Chl *a* values (Figs. 4d–f, 5c,d, 6d–f). Similarly, the senescence index values were also very low (most stations with values below 1%) throughout the study region. However, a slight tendency to higher values was found toward the surface (Figs. 4e,f, 6d,e).

Phytoplankton response to environmental drivers

The multivariate analysis showed a strong association between phytoplankton groups and physicochemical properties of seawater (Fig. 7). A Monte Carlo *F*-ratio test showed that nine environmental variables significantly ($p < 0.01$) contributed to explain the spatial distribution of phytoplankton groups: UMLD, stability, %MW, Chl *a*, temperature, salinity, DIN, phosphate, and silicic acid. The first two ordination CCA axes explained 55.9% of the total phytoplankton variance (35.9% and 20% in the first and second canonical axes, respectively) and 92.2% of the variance associated with the phytoplankton–environment relationship (59.2% and 33% in the first and second canonical axes, respectively).

The first CCA axis revealed a notable separation between diatoms and dinoflagellates and, consequently, between Gerlache and Bellingshausen stations (Fig. 7). The latter was mainly positively associated with stability, %MW, DIN, and phosphate. The analysis also indicated that diatoms were positively associated with both silicic acid and Chl *a* and negatively associated with UMLD. Dinoflagellates were positively associated with higher stability, %MW, and nutrients (DIN and phosphate), and negatively associated with both salinity and UMLD. The second axis indicated that minor groups (e.g., *P. antarctica*, green flagellates, and cryptophytes), which were more representative in Bransfield stations (Fig. 7), were positively correlated with both UMLD and salinity, and negatively associated with most of the other variables.

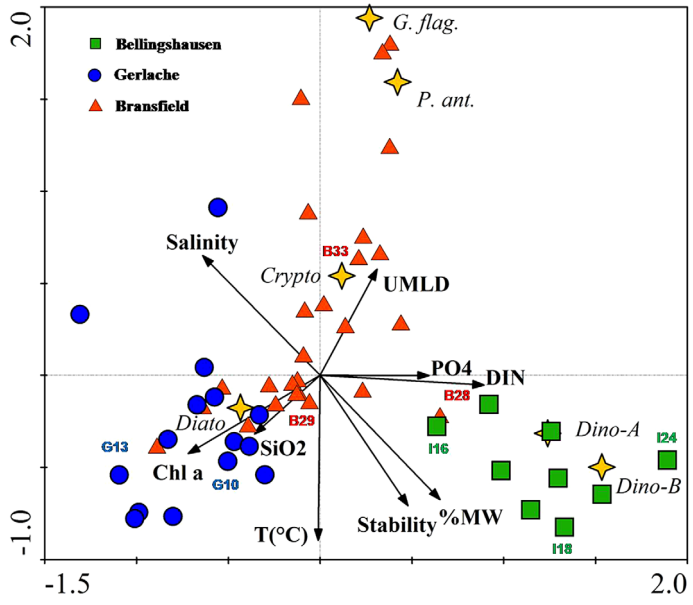

Fig. 7. Canonical correspondence analysis ordination diagram of absolute contributions of different phytoplankton groups at sea surface. The first two ordination axes represented 55.9% of the total phytoplankton group's variance and 92.2% of the phytoplankton–environment relationships. Arrows indicate explanatory variables [mean water column stability (Stability), UMLD, and sea surface temperature (*T*), Salinity, Chl *a*, %MW and DIN, phosphate (PO_4), and silicic acid (SiO_2)]. Yellow crosses refer to absolute contributions of phytoplankton groups. Crypto, cryptophytes; Dino-A, dinoflagellates Type a; Dino-B, dinoflagellates Type B; Diato, diatoms; P. ant., *Phaeocystis antarctica*; G. flag., green flagellates. Symbols and colors represent stations from different data sets (blue circles = Gerlache region; red triangle = Bransfield region; green square = Bellingshausen region). Stas. I16, I18, I24, G10, G13, B28, B29, and B33 are labeled because they represent very distinct environmental and biological conditions and their vertical profiles of environmental setting and phytoplankton composition are shown in Figs. 4–6.

Influence of phytoplankton Chl *a* biomass and community size structure on the CO_2 dynamics

A daily CO_2 net sink of –25.8 mmol m^{-2} d^{-1} was estimated for the study area, probably driven by the high phytoplankton Chl *a* biomass mainly dominated by large centric diatoms. The highest Chl *a* values, associated with higher diatom concentrations (*see* Fig. 3a,b), were related to the highest negative CO_2 sea–air fluxes

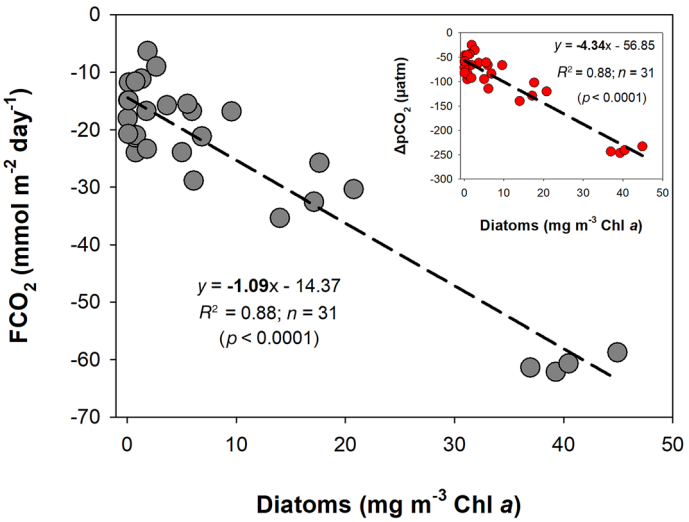

Fig. 8. Relationship between absolute contribution of diatoms (as Chl *a* concentration) and sea–air CO_2 flux (FCO_2) and ΔpCO_2 (i.e., the difference between seawater and atmospheric CO_2 partial pressures; inset figure). The negative values of FCO_2 indicate a net sea–air flux from atmosphere toward the ocean. The equations of the linear regressions (black dashed lines), the determination coefficient (R^2), the number (*n*) of samples and the *p*-values (*p*) are indicated.

(Fig. 8). The FCO_2 highest negative average value of −34.5 mmol m^{-2} d^{-1} was found in Gerlache Strait, followed by an intermediate mean value in Bransfield (−23.6 mmol m^{-2} d^{-1}), and the lowest in Bellinghausen (−17.8 mmol m^{-2} d^{-1}) (Supporting Information Table S4).

A closer examination of the correlation between Chl *a* vs. FCO_2, using 10 representative oceanographic stations of the subregions investigated, showed all stations featured negative FCO_2 values (Fig. 9a). However, the most negative levels exceeding −60.0 mmol m^{-2} d^{-1} were recorded at Stas. G10 and G13 in the Gerlache Strait. This was associated with the massive diatom bloom in the area (*see* Fig. 3b). Moreover, the higher values of Chl *a* biomass were characterized by high microphytoplankton (> 20 μm) contributions (Fig. 9b), with diatoms as the largest contributors to this size fraction (Fig. 9c). In contrast, the stations with lower Chl *a* values contained significant contributions of both picophytoplankton (0.7–2 μm) and nanophytoplankton (2–20 μm) fractions, followed by minimum microphytoplankton content. In addition to diatoms, the picophytoplankton and nanophytoplankton fractions had significant contributions from other groups such as dinoflagellates-B (e.g., Sta. I18) and/or green flagellates (e.g., Sta. G13) (Fig. 9c).

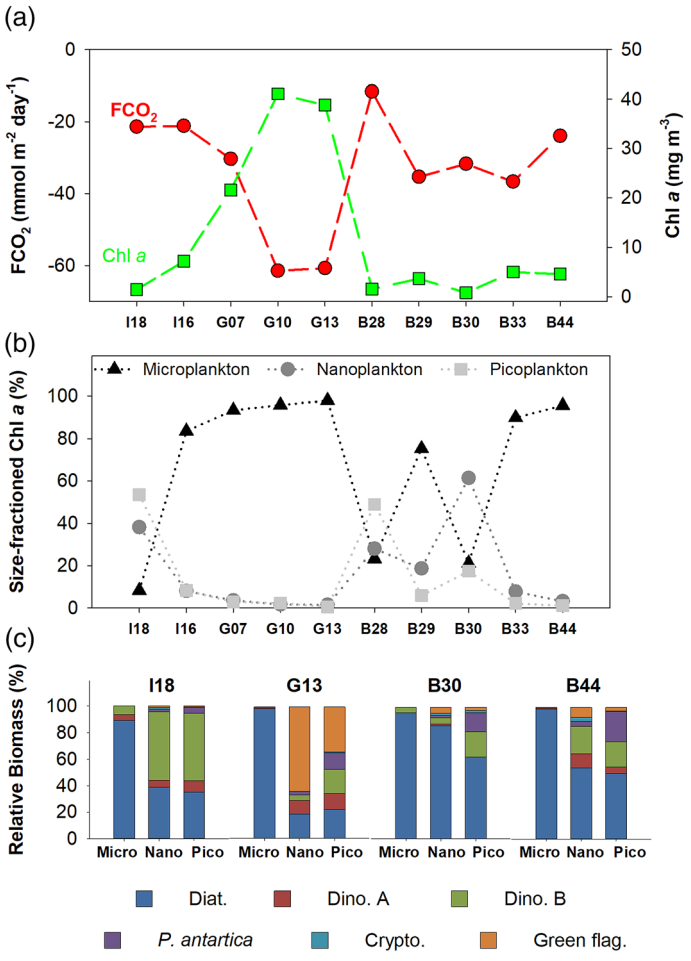

Fig. 9. Relationships between total Chl *a* and carbon flux (FCO_2) at surface for 10 representative stations of the study region (**a**) and their respective size fractionated Chl *a* (%) of microplankton, nanoplankton, and picoplankton (**b**) associated with relative biomass of phytoplankton groups (as Chl *a* concentration) for each station from the 10 selected stations (**c**).

Discussion

The Southern Ocean, in general, is characterized by high-nutrient and low-chlorophyll levels due to primary production limitation associated mainly with iron scarcity (Boyd et al. 2007), but also grazing (Smetacek et al. 2004) and light limitation (Mitchell and Holm-Hansen 1991; Nelson and Smith 1991). Nonetheless, high phytoplankton biomass has been found in particular regions, including coastal and shelf areas around the NAP (Prézelin et al. 2000; Arrigo et al. 2008; Mendes et al. 2012).

To our knowledge, this is the first study reporting a massive large-scale diatom bloom composed by the large diatom *O. weissflogii* throughout the NAP. Previous studies along the NAP have already reported the occurrence of *O. weissflogii* (e.g., Rodriguez et al. 2002; Varela et al. 2002; Garibotti et al. 2003; Mendes et al. 2012, 2013; Detoni et al. 2015; Mascioni et al. 2019; Nunes et al. 2019), but their records were almost always spatially punctual and associated with relatively low biomass, that is, with a little contribution of *O. weissflogii* to total phytoplankton biomass. In the present study, the low grazing pressure, estimated as pigment degradation products, may have contributed to sustaining the high Chl *a* biomass levels observed, particularly in both Gerlache and Bransfield Straits, during the study period. Macronutrients were highly abundant and although micronutrients such as iron (Fe) may be limiting productivity, the Antarctic Peninsula continental shelves have been depicted as a significant source of dissolved Fe to the upper ocean (Ardelan et al. 2010; Hatta et al. 2013; Annett et al. 2017; Sherrell et al. 2018; Jiang et al. 2019), not limiting phytoplankton growth even during intense blooms (Bown et al. 2017).

Distinct phytoplankton communities observed along the NAP, shifting the predominance between large diatoms to small dinoflagellates and other flagellates, were well recognized in the CCA diagram (Fig. 7), where the diatoms stand out as main contributors to the high Chl *a* values. We suggest that biological productivity along the NAP was primarily controlled by light availability and/or sedimentation processes, as a function of upper water column stability. Furthermore, sea ice, especially the timing of retreat, is an important driver to development of distinct phytoplankton assemblages due to its influence upon the water column stratification (Garibotti et al. 2003; Höfer et al. 2019). In fact, during the study period, the high percent of meltwater originated from the Bellingshausen Sea has strongly influenced the water column stability, generating a horizontally well-marked gradient between the three regions (*see* Fig. 2b) and, consequently, generating diverse phytoplankton assemblages and size structure.

Influence of UMLD and stability on diatom Chl *a* biomass distribution

There have been several previous studies along the Antarctic Peninsula during the spring and summer, including the NAP, which have recorded phytoplankton blooms composed by large (> 20 μm) diatoms (Garibotti et al. 2003; Vernet et al. 2008; Schloss et al. 2014; Schofield et al. 2017; Höfer et al. 2019). The high Chl *a* concentrations observed in the continental shelf areas during the spring and early summer are usually promoted by water column stability associated with low-density water around the melting ice (Alvain et al. 2008; Arrigo et al. 2008). The role of water column stability, jointly with shallower UMLD, has been recognized as an important driver to diatom blooms because it allows favorable conditions of nutrients supply and/or light intensity (Garibotti et al. 2003, 2005; Vernet et al. 2008; Petrou et al. 2016; Höfer et al. 2019; Prend et al. 2019). Similarly, the late summer diatom bloom showed here reached a biomass of 45 mg Chl *a* m^{-3} in Gerlache and was associated with a water column structure characterized by intermediate stability values ranging from 3.58 to 5.45 $\times 10^{-6}$ rad^2 m^{-1} and a shallower UMLD ranging between 20 and 37 m. A diatom-dominated system was also observed in the Bransfield Strait but with lower Chl *a* biomass, which was associated with deeper UMLD linked with lower water column stability. This dichotomy pattern is probably because the Bransfield Strait is a region of intensive mixture and mesoscale variability, under the influence of distinct water masses sourced from both the Bellingshausen and the Weddell seas (Sangrà et al. 2011; Gonçalves-Araujo et al. 2015).

As observed in previous studies (e.g., Garibotti et al. 2005; Montes-Hugo et al. 2009; Schofield et al. 2018), in our work, the UMLD has played an important role on phytoplankton community composition and Chl *a* biomass. For instance, under conditions of very shallow UMLD (< 15 m) and relatively strong pycnocline (e.g., between the Anvers and Brabant islands), there was a sharp decline in diatom Chl *a* biomass as they were replaced by nanoplankton such as cryptophytes. Several studies have highlighted an increasing contribution of cryptophytes to the NAP phytoplankton composition, including the Gerlache and Bransfield Straits (e.g., Mendes et al. 2013, 2018*a*,*b*; Gonçalves-Araujo et al. 2015). Some studies attributed their smaller size to changes from Antarctic krill-based toward salp-based food web (Atkinson et al. 2004; Moline et al. 2004; Montes-Hugo et al. 2009). The dominance of cryptophytes over diatoms in the NAP region has previously been attributed to sedimentation of large diatoms (Castro et al. 2002), advection of organism (Moline and Prézelin 1996), selective grazing (Garibotti et al. 2003), iron availability (Mendes et al. 2013), preference/physiological tolerance of cryptophytes to lower salinity waters (Moline et al. 2004), and/or due to a particular ability of those small flagellates to successfully grow in highly illuminated conditions in shallow upper mixed layers and strong water column stratification (Mendes et al. 2018*a*,*b*). However, during the late summer of 2016, only two sites (not shown) revealed significant contributions of cryptophytes to the phytoplankton community, which can indicate that conditions during the survey were not particularly favorable for the development of these small flagellates.

Conversely, a low-biomass community composed by small flagellates (mainly *P. antarctica* and green flagellates) was observed at stations influenced by cold waters from Weddell Sea origin in the Bransfield Strait. The CCA associated such pattern with a deeper UMLD (Fig. 7), presumably leading to light limitation (Smith and Nelson 1986; Prézelin et al. 2000; Petrou et al. 2016). On the other hand, as already stated above, a shift from diatoms to dinoflagellates (mainly small Gymnodiniales), followed a well-marked stability gradient under similar UMLD in the Bellingshausen Sea (Fig. 4). This pattern indicates that stability was also an important factor for the development and support of diatoms biomass (Fig. 7). We hypothesize that a thick (40–50 m) layer of stable water just below the UMLD (Fig. 5a,b) constitutes an effective/strong barrier that allows the large diatoms (mainly *O. weissflogii*) to endure for longer periods of time under favorable conditions. Such situation prevents the rapid sedimentation of diatoms and enables the development of a massive bloom as observed in the Gerlache Strait. In turn, the presence of only one thin layer of high stability (Fig. 4a–c) cannot hold the diatoms on the surface illuminated layers for a long period, promoting their rapid sinking (this condition is illustrated in Figs. 4d, 6d). Thus, a highly stable thin layer condition has allowed a gradual dominance by dinoflagellates over diatoms (Fig. 4e,f), given that dinoflagellates are able to move through the water column due to their flagella (Margalef et al. 1979).

O. weissflogii is characterized as a well-adapted species to stratified water columns, and their blooms are sustained by a shallow UMLD associated with coastal areas relatively sheltered from winds (Detoni et al. 2015). Another study in the western Antarctic Peninsula also found that phytoplankton growth rates were directly related with changes in water column stability and wind speed (Höfer et al. 2019). The authors showed that the faster phytoplankton growth rates were associated with weak winds in sheltered Antarctic coastal ecosystems. Therefore, given that Gerlache Strait is a relatively confined region characterized by coastal and sheltered waters, the massive diatom biomass recorded in our study suggest that the strait is a potential diatom bloom hotspot, in agreement with previous studies (e.g., Holm-Hansen et al. 1989; Serret et al. 2001; Rodríguez et al. 2002; Varela et al. 2002).

The role of diatoms on the biogeochemistry and marine ecosystem of the NAP

Because phytoplankton supports oceanic food webs and play a key role on the marine ecosystem's resilience, its abundance and composition may have a direct effect on the whole regional ecosystem with respect to the energy transfer through

food webs and the biological pump (Dubischar and Bathmann 1997; Smetacek et al. 2004; Salter et al. 2012; Assmy et al. 2013; Siegel et al. 2014; Rigual-Hernández et al. 2015). Recent studies have shown a positive association between upper ocean water column stability, phytoplankton dynamics, and FCO_2 from the atmosphere toward the ocean in summer (Jones et al. 2017; Kerr et al. 2018*a*; Brown et al. 2019). Nearly half of the oceanic CO_2 uptake occurs in the Southern Ocean (Takahashi et al. 2012). Within the biological compartment, diatoms are featured as the main contributors to the CO_2 uptake efficiency in relation to other phytoplankton, such as cryptophytes (Brown et al. 2019). Indeed, in our study, phytoplankton Chl *a* biomass was positively associated with diatoms and inversely related with FCO_2, that is, higher negative FCO_2 occurred at the center of the diatom bloom in the Gerlache Strait (Fig. 9). These data indicate a critical role of diatoms in driving oceanic CO_2 uptake, agreeing with other studies from different areas of the Antarctic Peninsula (Brown et al. 2019 and references therein). It is noteworthy, in the present study, that certain conditions such as a thick stability layer can enable the produced biomass to remain for a period of time near the surface, temporarily restricting the carbon sinking process. However, that condition may shift due to changes in water column structure dynamics, leading to particulate carbon export to depth.

In general, the Gerlache Strait is depicted as a hotspot of net sink of CO_2 (Kerr et al. 2018*b*), showing an estimated average (from 1999 to 2017) CO_2 flux of -12 ± 12.6 mmol m^{-2} d^{-1} during summer (Monteiro et al. 2020). This has also been reported by previous studies in association with diatom blooms (Álvarez et al. 2002; Varela et al. 2002). Based on our results, the intense *O. weissflogii* bloom recorded during February 2016 was the main driver generating a high carbon flux into the ocean, reaching nearly fivefold (approximately -62.1 mmol m^{-2} d^{-1}; Supporting Information Table S4) the average value for the region. On the other hand, Kerr et al. (2018*a*) recorded in early February 2015 a strong net flux of CO_2 to the atmosphere (16.7 ± 14.9 mmol m^{-2} d^{-1}) in Gerlache Strait, associated with an intrusion of relatively warm and salty waters in the region and a phytoplankton community dominated by cryptophytes. Therefore, differences in CO_2 behavior are likely associated with the changes in the dominant phytoplankton group, since small flagellates (e.g., cryptophytes) are less efficient in absorbing CO_2 and exporting organic carbon when compared to larger size diatoms (Jin et al. 2006; Gao and Campbell 2014).

Diatoms contribute to the biological pump through sinking from sunlit layers to the deep ocean. This process can occur (1) directly due to aggregates formation of entangled cells and chains with fast sinking rates (Smetacek et al. 2012) and/or (2) indirectly through fecal pellets produced by the zooplankton community (Manno et al. 2015). Interestingly, in the present study, in some vertical profiles (e.g., Figs. 4d, 6d) an evident DCM was observed close to 80–100 m depth. However, these maxima of diatoms-associated biomass seemed to be related to fast-sinking processes rather than to a more classical DCM because these peaks were at layers far below the Z_{eu}. Additionally, in these sites, it was possible to observe the formation of a relatively stable thin layer directly below the UMLD, similarly to that reported above for stations dominated by dinoflagellates, but with much lower stability values (Figs. 4a, 6a), probably allowing the bloom to sink. Additionally, the relative content of Chl *a* degradation products indicative of grazing on the phytoplankton population (Jeffrey et al. 1997) was low (grazing index below 5%) in all regions (Figs. 4–6). In the Southern Ocean, this grazing index has been found to be greater than 10% when associated with diatom blooms (e.g., Mendes et al. 2012; Pillai et al. 2018), indicating the prevalence of active grazing pressure during these high biomass events. However, mean Chl *a* in this study was approximately 10-fold higher in Gerlache than in the other regions, which would indicate a high phytoplankton growth rate and, therefore, a higher grazing rate would be expected in the area (e.g., Gutiérrez-Rodríguez et al. 2009). A possible explanation for this apparent discrepancy resides in the phytoplankton composition, which were massively dominated by large (mostly > 70 μm in length) centric diatoms during this survey. The large size of *O. weissflogii* probably resulted in reduced efficiency of zooplankton grazing, including the Antarctic krill (Quetin and Ross 1985; Opaliński et al. 1997; Haberman et al. 2003). Furthermore, the low senescence index values (Figs. 4–6) related to Chl *a*, indicated that diatom cells were healthy. This fact associated with low observed ciliates abundance in the microscopic analysis emphasizes the idea of a low grazing activity and/or viral lysis. Lastly, the large *O. weissflogii* size associated with their high Chl *a* biomass may have increased the efficiency of CO_2 uptake as well as fast sinking rates.

Final remarks

The low grazing indices and the high diatom biomass observed below the UMLD in the NAP (Figs. 4d, 6d) suggest that the diatom bloom, although apparently healthy, was in a fast sinking process. Probably, the production of cell aggregates may have helped to increase the sinking rates through the stabilized thin layer (Boyd and Newton 1999; Smetacek et al. 2012; Rigual-Hernández et al. 2019). These observations corroborate the concept that highly productive Antarctic coastal marine ecosystems are effective biological carbon pump systems, functioning as important sinking areas for atmospheric CO_2 (e.g., Ducklow et al. 2007; Arrigo et al. 2008). Conversely, this scenario of very large diatoms associated with low grazing pressure represents a low energy input from the primary producers to the classic short diatom–krill–whale Antarctic food chain.

Given that Antarctic marine organisms are dependent on sea ice dynamics, the associated physical changes that have been previously reported along the Antarctic Peninsula have

resulted in alterations of marine food webs across all trophic levels. In the base of the food web, phytoplankton changes have been shown to vary with latitude, with increasing Chl *a* trends in the southern sector contrasting with decreasing trends northward, namely, in the NAP. These current alterations have led to shifts in phytoplankton community composition with a smaller fraction of diatoms and/or large cells in the northern sector (Montes-Hugo et al. 2009; Schofield et al. 2010; Brown et al. 2019). In fact, recent studies along the NAP have registered the increasing importance of cryptophytes-dominated waters in shallow mixed layers (Mendes et al. 2013, 2018*a*; Gonçalves-Araujo et al. 2015; Kerr et al. 2018*a*). However, we detected here an intense diatom bloom composed by large cells that spanned a vast area of the NAP during late summer 2016, along with a high oceanic CO_2 uptake. This was likely associated with an atypical lag period in sea ice retreat caused by the first extreme El Niño of the 21st century (Santoso et al. 2017). This very strong 2015/2016 El Niño event likely promoted cold and weak southerly winds blow across the region, resulting in high sea ice concentrations advected on previous seasons. Such condition possibly decreased wind-induced mixing processes and increased the supply of meltwater in spring/summer due to the sea ice melting, which along with glacial meltwater stabilizes the upper ocean, supporting large phytoplankton blooms (Brown et al. 2019 and references therein).

Finally, although our results indicate an opposite trend of phytoplankton recent changes in the NAP region, our data are certainly restricted in temporal terms. Therefore, further investigations in this region including medium-term continuum studies are necessary to assess whether diatom blooms of that magnitude are frequent and ephemeral, and/or anomalously associated with large-scale climate modes of variability, such as conditions driven by Southern Annular Mode and/or El Niño.

References

Ackley, S. F., K. R. Buck, and S. Taguchi. 1979. Standing crop of algae in the sea ice of Weddell Sea region. Deep-Sea Res. Part I Oceanogr. Res. Pap. **26**: 269–281. doi:10.1016/0198-0149(79)90024-4

Alvain, S., C. Moulin, Y. Dandonneau, and H. Loisel. 2008. Seasonal distribution and succession of dominant phytoplankton groups in the global ocean: A satellite view. Global Biogeochem. Cycles **22**: GB3001. doi:10.1029/2007GB003154

Álvarez, M., A. F. Ríos, and G. Rosón. 2002. Spatio-temporal variability of air–sea fluxes of carbon dioxide and oxygen in the Bransfield and Gerlache Straits during Austral summer 1995–96. Deep-Sea Res. Part II Top. Stud. Oceanogr. **49**: 643–662. doi:10.1016/S0967-0645(01)00116-3

Aminot, A., and M. Chaussepied. 1983. Manuel des analyses chimiques en milieu marin. Brest, France: Centre National pour L'Exploitation des Oceans (CNEXO).

Annett, A. L., J. N. Fitzsimmons, M. J. Séguret, M. Lagerström, M. P. Meredith, O. Schofield, and R. M. Sherrell. 2017. Controls on dissolved and particulate iron distributions in surface waters of the Western Antarctic Peninsula shelf. Mar. Chem. **196**: 81–97. doi:10.1016/j.marchem.2017.06.004

Araujo, M. L. V., C. R. B. Mendes, V. M. Tavano, C. A. E. Garcia, and M. O. N. Baringer. 2017. Contrasting patterns of phytoplankton pigments and chemotaxonomic groups along 30°S in the subtropical South Atlantic Ocean. Deep-Sea Res. Part I Oceanogr. Res. Pap. **120**: 112–121. doi:10.1016/j.dsr.2016.12.004

Ardelan, M. V., O. Holm-Hansen, C. D. Hewes, C. S. Reiss, N. S. Silva, H. Dulaiova, E. Steinnes, and E. Sakshaug. 2010. Natural iron enrichment around the Antarctic Peninsula in the Southern Ocean. Biogeosciences **7**: 11–25.

Armbrust, E. V. 2009. The life of diatoms in the world's oceans. Nature **459**: 185–192. doi:10.1038/nature08057

Arrigo, K. R., D. H. Robinson, D. L. Worthen, R. B. Dunbar, G. R. DiTullio, M. VanWoert, and M. P. Lizotte. 1999. Phytoplankton community structure and the drawdown of nutrients and CO_2 in the Southern Ocean. Science **283**: 365–367. doi:10.1126/science.283.5400.365

Arrigo, K. R., G. L. van Dijken, and S. Bushinsky. 2008. Primary production in the Southern Ocean, 1997–2006. J. Geophys. Res. Oceans **113**: C08004. doi:10.1029/2007JC004551

Assmy, P., et al. 2013. Thick-shelled, grazer-protected diatoms decouple ocean carbon and silicon cycles in the iron-limited Antarctic Circumpolar Current. Proc. Natl. Acad. Sci. **110**: 20633–20638. doi:10.1073/pnas.1309345110

Atkinson, A., V. Siegel, E. Pakhomov, and P. Rothery. 2004. Long-term decline in krill stock and increase in salps within the Southern Ocean. Nature **432**: 100–103. doi:10.1038/nature02996

Bown, J., P. Laan, S. Ossebaar, K. Bakker, P. Rozema, and H. J. W. de Baar. 2017. Bioactive trace metal time series during Austral summer in Ryder Bay, Western Antarctic Peninsula. Deep-Sea Res. Part II Top. Stud. Oceanogr. **139**: 103–119. doi:10.1016/j.dsr2.2016.07.004

Boyd, P. W., and P. P. Newton. 1999. Does planktonic community structure determine downward particulate organic carbon flux in different oceanic provinces? Deep-Sea Res. Part I Oceanogr. Res. Pap. **46**: 63–91. doi:10.1016/S0967-0637(98)00066-1

Boyd, P. W., and others. 2007. Mesoscale iron enrichment experiments 1993–2005: Synthesis and future directions. Science **315**: 612–617. doi:10.1126/science.1131669

Brown, M. S., D. R. Munro, C. J. Feehan, C. Sweeney, H. W. Ducklow, and O. M. Schofield. 2019. Enhanced oceanic CO_2 uptake along the rapidly changing West Antarctic Peninsula. Nat. Clim. Change **9**: 678–683. doi:10.1038/s41558-019-0552-3

Carvalho, A. C. O., C. R. B. Mendes, R. Kerr, J. L. L. de Azevedo, F. Galdino, and V. M. Tavano. 2019. The impact of mesoscale eddies on the phytoplankton community in the South Atlantic Ocean: HPLC-CHEMTAX approach. Mar. Environ. Res. **144**: 154–165. doi:10.1016/j.marenvres.2018.12.003

Castro, C. G., A. F. Ríos, M. D. Doval, and F. F. Pérez. 2002. Nutrient utilisation and chlorophyll distribution in the Atlantic sector of the Southern Ocean during Austral summer 1995–96. Deep-Sea Res. Part II Top. Stud. Oceanogr. **49**: 623–641. doi:10.1016/S0967-0645(01)00115-1

Couto, N., D. G. Martinson, J. Kohut, and O. Schofield. 2017. Distribution of upper circumpolar deep water on the warming continental shelf of the West Antarctic peninsula. J. Geophys. Res. Oceans **122**: 5306–5315. doi:10.1002/2017JC012840

Dalla Rosa, L., E. R. Secchi, Y. G. Maia, A. N. Zerbini, and M. P. Heide-Jørgensen. 2008. Movements of satellite-monitored humpback whales on their feeding ground along the Antarctic Peninsula. Polar Biol. **31**: 771–781. doi:10.1007/s00300-008-0415-2

de Boyer Montégut, C., G. Madec, A. S. Fischer, A. Lazar, and D. Iudicone. 2004. Mixed layer depth over the global ocean: An examination of profile data and a profile based climatology. J. Geophys. Res. **109**: C12003. doi:10.1029/2004JC002378

Detoni, A. M. S., M. S. de Souza, C. A. E. Garcia, V. M. Tavano, and M. M. Mata. 2015. Environmental conditions during phytoplankton blooms in the vicinity of James Ross Island, east of the Antarctic Peninsula. Polar Biol. **38**: 1111–1127. doi:10.1007/s00300-015-1670-7

Dickson, A. G. 1990. Thermodynamics of the dissociation of boric acid in synthetic seawater from 273.15 to 318.15 K. Deep-Sea Res. Part I Oceanogr. Res. Pap. **37**: 755–766. doi:10.1016/0198-0149(90)90004-F

Dickson, A. G., J. D. Afghan, and G. C. Anderson. 2003. Reference materials for oceanic CO_2 analysis: A method for the certification of total alkalinity. Mar. Chem. **80**: 185–197. doi:10.1016/S0304-4203(02)00133-0

Dickson, A. G., C. L. Sabine, and J. R. Christian. 2007. Guide to best practices for ocean CO_2 measurements, p. 191. PICES Special Pubication 3. Marine Science Organization.

Dierssen, H. M., R. C. Smith, and M. Vernet. 2002. Glacial meltwater dynamics in coastal waters west of the Antarctic Peninsula. PNAS **99**: 1790–1795. doi:10.1073/pnas.032206999

Dlugokencky, E. J., P. M. Lang, K. A. Masarie, A. M. Crotwell, and M. J. Crotwell. 2015. Atmospheric carbon dioxide dry air mole fractions from the NOAA ESRL Carbon Cycle Cooperative Global Air Sampling Network, 1968–2014, version: 2015-09-08. https://oceaninformatics.ucsd.edu/datazoo/catalogs/pallter/datasets

Dubischar, C. D., and U. V. Bathmann. 1997. Grazing impacts of copepods and salps on phytoplankton in the Atlantic sector of the Southern Ocean. Deep-Sea Res. Part II Top. Stud. Oceanogr. **44**: 415–433. doi:10.1016/S0967-0645(96)00064-1

Ducklow, H. W., K. Baker, D. G. Martinson, L. B. Quetin, R. M. Ross, R. C. Smith, S. E. Stammerjohn, M. Vernet, and W. Fraser. 2007. Marine pelagic ecosystem: The West Antarctic Peninsula. Phil. Trans. R. Soc. B Biol. Sci. **362**: 67–94. doi:10.1098/rstb.2006.1955

Falkowski, P. G., R. T. Barber, and V. Smetacek. 1998. Biogeochemical controls and feedbacks on ocean primary production. Science **281**: 200–206. doi:10.1126/science.281.5374.200

Ferreira, A., A. M. Ciotti, C. R. B. Mendes, J. Uitz, and A. Bricaud. 2017. Phytoplankton light absorption and the package effect in relation to photosynthetic and photoprotective pigments in the northern tip of Antarctic Peninsula. J. Geophys. Res. **122**: 7344–7362. doi:10.1002/2017JC012964

Gao, K., and D. A. Campbell. 2014. Photophysiological responses of marine diatoms to elevated CO2 and decreased pH: A review. Funct. Plant Biol. **41**: 449–459. doi:10.1071/FP13247

Garibotti, I. A., M. Vernet, M. E. Ferrario, R. C. Smith, R. M. Ross, and L. B. Quetin. 2003. Phytoplankton spatial distribution patterns along the western Antarctic Peninsula (Southern Ocean). Mar. Ecol. Prog. Ser. **261**: 21–39. doi:10.3354/meps261021

Garibotti, I. A., M. Vernet, R. C. Smith, and M. E. Ferrario. 2005. Interannual variability in the distribution of the phytoplankton standing stock across the seasonal sea-ice zone west of the Antarctic Peninsula. J. Plankton Res. **27**: 825–843. doi:10.1093/plankt/fbi056

Goeyt, C., and A. Poisson. 1989. New determination of carbonic acid dissociation constants in seawater as a function of temperature and salinity. Deep-Sea Res. Part I Oceanogr. Res. Pap. **36**: 1635–1654. doi:10.1016/0198-0149(89)90064-2

Gonçalves-Araujo, R., M. S. de Souza, V. M. Tavano, and C. A. E. Garcia. 2015. Influence of oceanographic features on spatial and interannual variability of phytoplankton in the Bransfield Strait. Antarctica. J. Marine Syst. **142**: 1–15. doi:10.1016/j.jmarsys.2014.09.007

Gutiérrez-Rodríguez, A., M. Latasa, B. Mourre, and E. A. Laws. 2009. Coupling between phytoplankton growth and microzooplankton grazing in dilution experiments: Potential artefacts. Mar. Ecol. Prog. Ser. **383**: 1–9. doi:10.3354/meps08005

Haberman, K. L., R. M. Ross, and L. B. Quetin. 2003. Diet of the Antarctic krill (*Euphausia superba* Dana): II selective grazing in mixed phytoplankton assemblages. J. Exp. Mar. Biol. Ecol. **283**: 97–113. doi:10.1016/S0022-0981(02)00467-7

Hatta, M., C. I. Measures, K. E. Selph, M. Zhou, and W. T. Hiscock. 2013. Iron fluxes from the shelf regions near the South Shetland Islands in the Drake Passage during the austral-winter 2006. Deep-Sea Res. Part II Top. Stud. Oceanogr. **90**: 89–101. doi:10.1016/j.dsr2.2012.11.003

Higgins, H. W., S. W. Wright, and L. Schlüter. 2011. Quantitative interpretation of chemotaxonomic pigment data, p. 257–313. *In* S. Roy, C. A. Llewellyn, E. S. Egeland, and G. Johnson [eds.], Phytoplankton pigments: Characterization, chemotaxonomy and applications in oceanography. Cambridge, UK: Cambridge Univ. Press.

Hillebrand, H., C. D. Dürselen, D. Kirschtel, U. Pollingher, and T. Zohary. 1999. Biovolume calculation for pelagic and benthic microalgae. J. Phycol. **35**: 403–424. doi:10.1046/j.1529-8817.1999.3520403.x

Höfer, J., R. Giesecke, M. J. Hopwood, V. Carrera, E. Alarcón, and H. E. González. 2019. The role of water column stability and wind mixing in the production/export dynamics of two bays in the Western Antarctic Peninsula. Prog. Oceanogr. **174**: 105–116. doi:10.1016/j.pocean.2019.01.005

Hooker, S. B., and others. 2005. The second sea-WiFS HPLC analysis round-robin experiment (SeaHARRE-2). NASA Tech. Memo. 2005–212785. Greenbelt, MD: NASA Goddard Space Flight Center.

Holm-Hansen, O., B. G. Mitchell, and C. D. Hewes. 1989. Phytoplankton blooms in the vicinity of Palmer station, Antarctica. Polar Biol. **10**: 49–57. doi:10.1007/BF00238290

Huot, Y., M. Babin, F. Bruyant, C. Grob, M. S. Twardowski, and H. Claustre. 2007. Relationship between photosynthetic parameters and different proxies of phytoplankton biomass in the subtropical ocean. Biogeosciences **4**: 853–868. doi:10.5194/bg-4-853-2007

Jeffrey, S. W. 1974. Profiles of photosynthetic pigments in the ocean using thin-layer chromatography. Mar. Biol. **26**: 101–110. doi:10.1007/BF00388879

Jeffrey, S. W., R. F. C. Mantoura, and S. W. Wright. 1997. Phytoplankton pigments in oceanography: Guidelines to modern methods. Paris: UNESCO.

Jiang, M., and others. 2019. Fe sources and transport from the Antarctic Peninsula shelf to the southern Scotia Sea. Deep-Sea Res. Part I Oceanogr. Res. Pap. **150**: 103060. doi:10.1016/j.dsr.2019.06.006

Jin, X., N. Gruber, J. P. Dunne, J. L. Sarmiento, and R. A. Armstrong. 2006. Diagnosing the contribution of phytoplankton functional groups to the production and export of particulate organic carbon, $CaCO_3$, and opal from global nutrient and alkalinity distributions. Global Biogeochem. Cycles **20**: GB2015. doi:10.1029/2005GB002532

Jones, E. M., M. Fenton, M. P. Meredith, N. M. Clargo, S. Ossebaar, H. W. Ducklow, H. J. Venables, and H. J. W. de Baar. 2017. Ocean acidification and calcium carbonate saturation states in the coastal zone of the West Antarctic Peninsula. Deep-Sea Res. Part II Top. Stud. Oceanogr. **139**: 181–194. doi:10.1016/j.dsr2.2017.01.007

Kerr, R., and others. 2018*a*. Carbonate system properties in the Gerlache Strait, Northern Antarctic Peninsula (February 2015): I. Sea–air CO_2 fluxes. Deep-Sea Res. Part II Top Stud. Oceanogr. **149**: 171–181. doi:10.1016/j.dsr2.2017.02.008

Kerr, R., and others. 2018*b*. Carbonate system properties in the Gerlache Strait, Northern Antarctic Peninsula (February 2015): II. Anthropogenic CO_2 and seawater acidification. Deep-Sea Res. Part II Top Stud. Oceanogr. **149**: 182–192. doi:10.1016/j.dsr2.2017.07.007

Kerr, R., M. M. Mata, C. R. B. Mendes, and E. R. Secchi. 2018*c*. Northern Antarctic Peninsula: A marine climate hotspot of rapid changes on ecosystems and ocean dynamics. Deep-Sea Res. Part II Top. Stud. Oceanogr. **149**: 4–9. doi:10.1016/j.dsr2.2018.05.006

Laika, H. E., C. Goyet, F. Vouve, A. Poisson, and F. Touratier. 2009. Interannual properties of the CO_2 system in the Southern Ocean south of Australia. Antarct. Sci. **21**: 663–680. doi:10.1017/S0954102009990319

Lewis, E., D. Wallace, and L. J. Allison. 1998. Program developed for CO_2 system calculations. Carbon Dioxide Information Analysis Center: Oak Ridge, TN, p. 38.

Lima, C. R., C. R. B. Mendes, V. M. Tavano, A. M. S. Detoni, and E. R. Secchi. 2019. Chemotaxonomy-based mapping of phytoplankton communities in the subtropical Southwestern Atlantic Ocean, with emphasis on the marine cyanobacterium *Trichodesmium*. Prog. Oceanogr. **172**: 77–88. doi:10.1016/j.pocean.2019.01.008

Mackey, M. D., D. J. Mackey, H. W. Higgins, and S. W. Wright. 1996. CHEMTAX—A program for estimating class abundances from chemical markers: Application to HPLC measurements of phytoplankton. Mar. Ecol. Prog. Ser. **144**: 265–283. doi:10.3354/meps144265

Mackey, D. J., H. W. Higgins, M. D. Mackey, and D. Holdsworth. 1998. Algal class abundances in the western equatorial pacific: Estimation from HPLC measurements of chloroplast pigments using CHEMTAX. Deep-Sea Res. Part I Oceanogr. Res. Pap. **45**: 1441–1468. doi:10.1016/S0967-0637(98)00025-9

Malviya, M. S., and others. 2016. Insights into global diatom distribution and diversity in the world's ocean. PNAS **113**: E1516–E1525. doi:10.1073/pnas.1509523113

Manno, C., G. Stowasser, P. Enderlein, S. Fielding, and G. A. Tarling. 2015. The contribution of zooplankton faecal pellets to deep carbon transport in the Scotia Sea (Southern Ocean). Biogeosciences **12**: 1955–1965. doi:10.5194/bg-12-1955-2015

Margalef, R., M. Estrada, and D. Blasco. 1979. Functional morphology of organisms involved in red tides, as adapted to decaying turbulence, p. 89–94. *In* D. L. Taylor and H. H. Seliger [eds.], Toxic dinoflagellate blooms. Proceedings of the Second International Conference on toxic dinoflagellate blooms. New York, NY: Elsevier.

Mascioni, M., G. O. Almandoz, A. O. Ciardelli, A. Cusick, M. E. Ferrario, and M. Vernet. 2019. Phytoplankton composition and bloom formation in unexplored nearshore waters of the western Antarctic Peninsula. Polar Biol. **42**: 1859–1872. doi:10.1007/s00300-019-02564-7

Massom, R. A., T. A. Scambos, L. G. Bennetts, P. Reid, V. A. Squire, and S. E. Stammerjohn. 2018. Antarctic ice shelf disintegration triggered by sea ice loss and ocean swell. Nature **558**: 383–389. doi:10.1038/s41586-018-0212-1

Mendes, C. R., P. Cartaxana, and V. Brotas. 2007. HPLC determination of phytoplankton and microphytobenthos pigments: Comparing resolution and sensitivity of a C18 and a C8 method. Limnol. Oceanogr. Methods **5**: 363–370. doi:10.4319/lom.2007.5.363

Mendes, C. R., C. Sá, J. Vitorino, C. Borges, V. M. T. Garcia, and V. Brotas. 2011. Spatial distribution of phytoplankton assemblages in the Nazare submarine canyon region (Portugal): HPLC-CHEMTAX approach. J. Mar. Syst. **87**: 90–101. doi:10.1016/j.jmarsys.2011.03.005

Mendes, C. R. B., M. S. de Souza, V. M. T. Garcia, M. C. Leal, V. Brotas, and C. A. E. Garcia. 2012. Dynamics of phytoplankton communities during late summer around the tip of the Antarctic Peninsula. Deep-Sea Res. Part I Oceanogr. Res. Pap. **65**: 1–14. doi:10.1016/j.dsr.2012.03.002

Mendes, C. R. B., V. M. Tavano, M. C. Leal, M. S. de Souza, V. Brota, and C. A. E. Garcia. 2013. Shifts in the dominance between diatoms and cryptophytes during three late summers in the Bransfield Strait (Antarctic Peninsula). Polar Biol. **36**: 537–547. doi:10.1007/s00300-012-1282-4

Mendes, C. R. B., R. Kerr, V. M. Tavano, F. A. Cavalheiro, C. A. E. Garcia, D. R. G. Dessai, and N. Anilkumar. 2015. Cross-front phytoplankton pigments and chemotaxonomic groups in the Indian sector of the Southern Ocean. Deep-Sea Res. Part II Top. Stud. Oceanogr. **118**: 221–232. doi:10.1016/j.dsr2.2015.01.003

Mendes, C. R. B., V. M. Tavano, R. Kerr, T. S. Dotto, T. Maximiano, and E. R. Secchi. 2018*a*. Impact of sea ice on the structure of phytoplankton communities in the northern Antarctic Peninsula. Deep-Sea Res. Part II Top. Stud. Oceanogr. **149**: 111–123. doi:10.1016/j.dsr2.2017.12.003

Mendes, C. R. B., V. M. Tavano, T. S. Dotto, R. Kerr, M. S. de Souza, C. A. E. Garcia, and E. R. Secchi. 2018*b*. New insights on the dominance of cryptophytes in Antarctic coastal waters: A case study in Gerlache Strait. Deep-Sea Res. Part II Top. Stud. Oceanogr. **149**: 161–170. doi:10.1016/j.dsr2.2017.02.010

Meredith, M. P., and J. C. King. 2005. Rapid climate change in the ocean west of the Antarctic Peninsula during the second half of the 20th century. Geophys. Res. Lett. **32**: L19604. doi:10.1029/2005GL024042

Mitchell, B. G., and O. Holm-Hansen. 1991. Observations of modeling of the Antartic phytoplankton crop in relation to mixing depth. Deep-Sea Res. Part I Oceanogr. Res. Pap. **38**: 981–1007. doi:10.1016/0198-0149(91)90093-U

Moline, M. A., and B. B. Prézelin. 1996. Palmer LTER 1991–1994: Long-term monitoring and analyses of physical factors regulating variability in coastal Antarctic phytoplankton biomass, in situ productivity and taxonomic composition over sub-seasonal, seasonal and interannual time scales. Mar. Ecol. Prog. Ser. **145**: 143–160. doi:10.3354/meps145143

Moline, M. A., H. Claustre, T. K. Frazer, O. Schofield, and M. Vernet. 2004. Alteration of the food web along the Antarctic Peninsula in response to a regional warming trend. Glob. Change Biol. **10**: 1973–1980. doi:10.1111/j.1365-2486.2004.00825.x

Monteiro, T., R. Kerr, I. B. M. Orselli, and J. M. Lencina-Avilaac. 2020. Towards an intensified summer CO_2 sink behaviour in the Southern Ocean coastal regions. Prog. Oceanogr. **183**: 102267. doi:10.1016/j.pocean.2020.102267

Montes-Hugo, M., S. C. Doney, H. W. Duclow, W. Fraser, D. Martinson, S. E. Stammerjohn, and O. Schofield. 2009. Recent changes in phytoplankton communities associated with rapid regional climate change along the Western Antarctic Peninsula. Science **323**: 1470–1473. doi:10.1126/science.1164533

Nelson, D. M., and W. O. Smith Jr. 1991. Sverdrup revisited: Critical depths, maximum chlorophyll levels, and the control of Southern Ocean productivity by the irradiance-mixing regime. Limnol. Oceanogr. **36**: 1650–1661. doi:10.4319/lo.1991.36.8.1650

Nowacek, D. P., and others. 2011. Super-aggregations of krill and humpback whales in Wilhelmina Bay, Antarctic Peninsula. Plos One **6**: e19173. doi:10.1371/journal.pone.0019173

Nunes, S., M. Latasa, M. Delgado, M. Emelianov, R. Simó, and M. Estrada. 2019. Phytoplankton community structure in contrasting ecosystems of the Southern Ocean: South Georgia, South Orkneys and western Antarctic Peninsula. Deep-Sea Res. Part I Oceanogr. Res. Pap. **151**: 103059. doi:10.1016/j.dsr.2019.06.005

Opaliński, K. W., K. Maciejewska, and L. V. Georgieva. 1997. Notes of food selection in the Antarctic krill *Euphausia superba*. Polar Bio. **17**: 350–357. doi:10.1007/PL00013376

Person, R., O. Aumont, and M. Lévy. 2018. The biological pump and seasonal variability of pCO_2 in the Southern Ocean: Exploring the role of diatom adaptation to low iron. J. Geophys. Res-Oceans. **123**: 3204–3226. doi:10.1029/2018JC013775

Petrou, K., S. A. Kranz, S. Trimborn, C. S. Hassler, S. B. Ameijeiras, O. Sackett, P. J. Ralph, and A. T. Davidson. 2016. Southern Ocean phytoplankton physiology in a changing climate. J. Plant Physiol. **203**: 135–150. doi:10.1016/j.jplph.2016.05.004

Pierrot, D., E. Lewis, and D. W. R. Wallace. 2006. MS excel program developed for CO_2 system calculations, ORNL/CDIAC-105a. Oak Ridge, TN: Carbon Dioxide Information Analysis Center. Oak Ridge National Laboratory, U.S. Department of Energy. doi:10.3334/CDIAC/otg.CO2SYS_XLS_CDIAC105a

Pillai, H. U. K., and others. 2018. Planktonic food web structure at SSTF and PF in the Indian sector of the Southern

Ocean during austral summer 2011. Polar Res. **37**: 1495545. doi:10.1080/17518369.2018.1495545

Pondaven, P., O. Ragueneau, P. Tréguer, A. Hauvespre, L. Dezileau, and J. L. Reyss. 2000. Resolving the "opal paradox" in the Southern Ocean. Nature **405**: 168–172.

Prend, C. J., S. T. Gille, L. D. Talley, B. G. Mitchell, I. Rosso, and M. R. Mazloff. 2019. Physical drivers of phytoplankton bloom initiation in the Southern Ocean's Scotia Sea. J. Geophys. Res-Oceans. **124**: 5811–5826. doi:10.1029/2019JC015162

Prézelin, B. B., E. E. Hofmann, C. Mengelt, and J. M. Klinck. 2000. The linkage between Upper Circumpolar Deep Water (UCDW) and phytoplankton assemblages on the west Antarctic Peninsula continental shelf. J. Mar. Res. **58**: 165–202. doi:10.1357/002224000321511133

Prézelin, B. B., E. E. Hofmann, M. Moline, and J. M. Klinck. 2004. Physical forcing of phytoplankton community structure and primary production in continental shelf waters of the Western Antarctic Peninsula. J. Mar. Res. **62**: 419–460. doi:10.1357/0022240041446173

Quetin, L. B., and R.M Ross. 1985. Feeding by Antarctic krill, *Euphausia superba*: Does size matter? P. 372-377. *In* W. R Siegfried, P.R Condy, R.M Laws [eds.], Antarctic nutrient cycles and food webs, Springer-Verlag, Berlin

Rigual-Hernández, A. S., T. W. Trull, S. G. Bray, A. Cortina, and L. K. Armand. 2015. Latitudinal and temporal distributions of diatom populations in the pelagic waters of the Subantarctic and Polar Frontal zones of the Southern Ocean and their role in the biological pump. Biogeosciences **12**: 8615–8690. doi:10.5194/bg-12-5309-2015

Rigual-Hernández, A. S., C. H. Pilskaln, A. Cortina, F. Abrantes, and L. K. Armande. 2019. Diatom species fluxes in the seasonally ice-covered Antarctic Zone: New data from offshore Prydz Bay and comparison with other regions from the eastern Antarctic and western Pacific sectors of the Southern Ocean. Deep-Sea Res. Part II Top. Stud. Oceanogr. **161**: 92–104. doi:10.1016/j.dsr2.2018.06.005

Rivaro, P., R. Messa, C. Ianni, E. Magi, and G. Budillon. 2014. Distribution of total alkalinity and pH in the Ross Sea (Antarctica) waters during austral summer 2008. Polar Res. **33**: 20403. doi:10.3402/polar.v33.20403

Rodriguez, F., M. Varela, and M. Zapata. 2002. Phytoplankton assemblages in the Gerlache and Bransfield Straits (Antarctic Peninsula) determined by light microscopy and CHEMTAX analysis of HPLC pigment data. Deep-Sea Res. Part II Top. Stud. Oceanogr. **49**: 723–747. doi:10.1016/S0967-0645(01)00121-7

Rodríguez, J., F. Jiménez-Gómez, J. M. Blanco, and F. L. Figueroa. 2002. Physical gradients and spatial variability of the size structure and composition of phytoplankton in the Gerlache Strait (Antarctica). Deep-Sea Res. Part II Top. Stud. Oceanogr. **49**: 693–706. doi:10.1016/S0967-0645(01)00119-9

Rousseaux, C., and W. Gregg. 2014. Interannual variation in phytoplankton primary production at a global scale. Remote Sens. (Basel) **6**: 1–19. doi:10.3390/rs6010001

Rozema, P. D., H. J. Venables, W. H. van de Poll, A. Clarke, M. P. Meredith, and A. G. J. Buma. 2017. Interannual variability in phytoplankton biomass and species composition in northern Marguerite Bay (West Antarctic Peninsula) is governed by both winter sea ice cover and summer stratification. Limnol. Oceanogr. **62**: 235–252. doi:10.1002/lno.10391

Salter, I., A. E. S. Kemp, C. M. Moore, R. S. Lampitt, G. A. Wolff, and J. Holtvoeth. 2012. Diatom resting spore ecology drives enhanced carbon export from a naturally iron-fertilized bloom in the Southern Ocean. Global Biogeochem. Cycles **26**: GB1014. doi:10.1029/2010GB003977

Sangrà, P., and others. 2011. The Bransfield current system. Deep-Sea Res. Part I Oceanogr. Res. Pap. **58**: 390–402. doi:10.1016/j.dsr.2011.01.011

Santoso, A., M. J. Mcphaden, and W. Cai. 2017. The defining characteristics of ENSO extremes and the strong 2015/2016 El Niño. Rev. Geophys. **55**: 1079–1129. doi:10.1002/2017RG000560

Schloss, I. R., and others. 2014. On the phytoplankton bloom in coastal waters of southern King George Island (Antarctica) in January 2010: An exceptional feature? Limnol. Oceanogr. **59**: 195–210. doi:10.4319/lo.2014.59.1.0195

Schlüter, L., P. Henriksen, T. G. Nielsen, and H. H. Jakobsen. 2011. Phytoplankton composition and biomass across the southern Indian Ocean. Deep-Sea Res. Part I Oceanogr. Res. Pap. **58**: 546–556. doi:10.1016/j.dsr.2011.02.007

Schlüter, L., F. Møhlenberg, H. Havskum, and S. Larsen. 2000. The use of phytoplankton pigments for identifying and quantifying phytoplankton groups in coastal areas: Testing the influence of light and nutrients on pigment/chlorophyll a ratios. Mar. Ecol. Prog. Ser. **192**: 49–63. doi:10.3354/meps192049

Schofield, O., H. W. Ducklow, D. G. Martinson, M. P. Meredith, M. A. Moline, and W. R. Fraser. 2010. How do polar marine ecosystems respond to rapid climate change? Science **328**: 1520–1523. doi:10.1126/science.1185779

Schofield, O., and others. 2017. Decadal variability in coastal phytoplankton community composition in a changing West Antarctic Peninsula. Deep-Sea Res. Part I Oceanogr. Res. Pap. **124**: 42–54. doi:10.1016/j.dsr.2017.04.014

Schofield, O., M. Brown, J. Kohut, S. Nardelli, G. Saba, N. Waite, and H. Ducklow. 2018. Changes in the upper ocean mixed layer and phytoplankton productivity along the West Antarctic Peninsula. Phil. Trans. R. Soc. A **376**: 20170173. doi:10.1098/rsta.2017.0173

Scott, F. J., and H. J. Marchant. 2005. Antarctic marine protists. Canberra: Australian Biological Resources Study and Australian Antarctic Division.

Secchi, E. R., L. Dalla Rosa, P. G. Kinas, R. F. Nicolette, A. M. N. Rufino, and A. F. Azevedo. 2011. Encounter rates and abundance of humpback whales (*Megaptera novaeangliae*) in Gerlache and Bransfield Straits, Antarctic Peninsula. J. Cetacean Res. Manage. **3**: 107–111.

Serret, P., E. Fernández, R. Anadón, and M. Varela. 2001. Trophic control of biogenic carbon export in Bransfield and Gerlache Straits. Antarctica. J. Plankton Res. **23**: 1345–1360. doi:10.1093/plankt/23.12.1345

Seyboth, E., S. Botta, C. R. B. Mendes, J. Negrete, L. Dalla Rosa, and E. R. Secchi. 2018. Isotopic evidence of the effect of warming on the northern Antarctic Peninsula ecosystem. Deep-Sea Res. Part II Top. Stud. Oceanogr. **149**: 218–228. doi:10.1016/j.dsr2.2017.12.020

Sherrell, R. M., A. L. Annett, J. N. Fitzsimmons, V. J. Roccanova, and M. P. Meredith. 2018. A "shallow bathtub ring" of local sedimentary iron input maintains the Palmer Deep biological hotspot on the West Antarctic Peninsula shelf. Philos. Trans. Roy. Soc. A Math. Phys. Eng. Sci. **376**: 2122. doi:10.1098/rsta.2017.0171

Siegel, D. A., K. O. Buesseler, S. C. Doney, S. F. Sailley, M. J. Behrenfeld, and P. W. Boyd. 2014. Global assessment of ocean carbon export by combining satellite observations and food-web models. Global Biogeochem. Cycles **28**: 181–196. doi:10.1002/2013GB004743

Smetacek, V., P. Assmy, and J. Henjes. 2004. The role of grazing in structuring Southern Ocean pelagic ecosystems and biogeochemical cycles. Antarct. Sci. **16**: 541–558. doi:10.1017/S0954102004002317

Smetacek, V., and others. 2012. Deep carbon export from a Southern Ocean iron-fertilized diatom bloom. Nature **487**: 313–319. doi:10.1038/nature11229

Smith, W. O. J., and D. M. Nelson. 1986. Importance of ice edge phytoplankton production in the Southern Ocean. Bioscience **36**: 251–257. doi:10.2307/1310215

Smith, R. C., and S. E. Stammerjohn. 2001. Variations of surface air temperature and sea-ice extent in the western Antarctic Peninsula region. Ann. Glaciol. **33**: 493–500. doi:10.3189/172756401781818662

Sournia, A. 1978. Phytoplankton manual. Paris: Muse'um National d'Histoire Naturelle, UNESCO.

Southwell, C., and others. 2012. A review of data on abundance, trends in abundance, habitat utilisation and diet for Southern Ocean ice-breeding seals. CCAMLR Sci **19**: 1–49 doi:10013/epic.40419.

Stammerjohn, S. E., D. G. Martinson, R. C. Smith, and R. A. Iannuzzi. 2008. Sea ice in the western Antarctic Peninsula region: Spatio-temporal variability from ecological and climate change perspectives. Deep-Sea Res. Part II Top. Stud. Oceanogr. **55**: 2041–2058. doi:10.1016/j.dsr2.2008.04.026

Takahashi, T., C. Sweeney, B. Hales, D. W. Chipman, T. Newberger, J. G. Goddard, R. A. Iannuzzi, and S. C. Sutherland. 2012. The changing carbon cycle in the Southern Ocean. Oceanography **25**: 26–37. doi:10.5670/oceanog.2012.71

Ter Braak, C. J. F., and I. C. Prentice. 1988. A theory of gradient analysis. Adv. Ecol. Res. **18**: 271–317. doi:10.1016/S0065-2504(08)60183-X

Tréguer, P., and others. 2017. Influence of diatom diversity on the ocean biological carbon pump. Nat. Geosci. **11**: 27–37. doi:10.1038/s41561-017-0028-x

Trivelpiece, W. Z., J. T. Hinke, A. K. Miller, C. S. Reiss, S. G. Trivelpiece, and G. M. Watters. 2011. Variability in krill biomass links harvesting and climate warming to penguin population changes in Antarctica. PNAS **108**: 7625–7628. doi:10.1073/pnas.1016560108

Turner, J., J. S. Hosking, T. Phillips, and G. J. Marshall. 2013. Temporal and spatial evolution of the Antarctic sea ice prior to the September 2012 record maximum extent. Geophys. Res. Lett. **40**: 5894–5898. doi:10.1002/2013GL058371

Turner, J., J. S. Hosking, T. J. Bracegirdle, G. J. Marshall, and T. Phillips. 2015. Recent changes in Antarctic sea ice. Phil. Trans. R. Soc. A **373**: 20140163. doi:10.1098/rsta.2014.0163

Uppstrom, L. R. 1974. Boron/chlorinity ratio of deep-sea water from the Pacific Ocean. Deep-Sea Res. **21**: 161–162. doi:10.1016/0011-7471(74)90074-6

Utermöhl, H. 1958. Zur Vervollkommnung der quantitativen phytoplankton Methodik. Mitt. Int. Ver. Theor. Angew. Limnol. **9**: 1–38. doi:10.1080/05384680.1958.11904091

Varela, M., E. Fernandez, and P. Serret. 2002. Size-fractionated phytoplankton biomass and primary production in the Gerlache and south Bransfield Straits (Antarctic Peninsula) in Austral summer 1995–1996. Deep-Sea Res. Part II Top. Stud. Oceanogr. **49**: 749–768. doi:10.1016/S0967-0645(01)00122-9

Vernet, M., D. Martinson, R. Iannuzzi, S. Stammerjohn, W. Kozlowski, K. Sines, R. Smith, and I. Garibotti. 2008. Primary production within the sea-ice zone west of the Antarctic peninsula: I—Sea ice, summer mixed layer, and irradiance. Deep-Sea Res. Part II Top. Stud. Oceanogr. **55**: 2068–2085. doi:10.1016/j.dsr2.2008.05.021

Wanninkhof, R. 2014. Relationship between wind speed and gas exchange over the ocean revisited. Limnol. Oceanogr. Methods. **12**: 351–362. doi:10.4319/lom.2014.12.351

Weiss, R. F. 1974. Carbon dioxide in water and seawater: The solubility of a non-ideal gas. Mar. Chem. **2**: 203–215. doi:10.1016/0304-4203(74)90015-2

Wright, S. W., A. Ishikawa, H. J. Marchant, A. T. Davidson, R. L. van den Enden, and G. V. Nash. 2009. Composition and significance of picophytoplankton in Antarctic waters. Polar Biol. **32**: 797–808. doi:10.1007/s00300-009-0582-9

Wright, S. W., R. L. van den Enden, I. Pearce, A. T. Davidson, F. J. Scott, and K. J. Westwood. 2010. Phytoplankton community structure and stocks in the Southern Ocean (30–80°E) determined by CHEMTAX analysis of HPLC

pigment signatures. Deep-Sea Res. Part II Top. Stud. Oceanogr. **57**: 758–778. doi:10.1016/j.dsr2.2009.06.015

Zapata, M., F. Rodríguez, and J. L. Garrido. 2000. Separation of chlorophylls and carotenoids from marine phytoplankton: A new HPLC method using a reversed phase C8 column and pyridine-containing mobile phases. Mar. Ecol. Prog. Ser. **195**: 29–45. doi:10.3354/meps195029

Acknowledgments

This is a multidisciplinary study as part of the Brazilian High Latitude Oceanography Group (GOAL) activities in the Brazilian Antarctic Program (PROANTAR). Financial support was provided by National Council for Research and Development (CNPq) and Coordination for the Improvement of Higher Education Personnel (CAPES). This study was conducted within the activities of the INTERBIOTA, NAUTILUS, PROVOCCAR, ECOPELAGOS (CNPq grant numbers 407889/2013-2, 405869/2013-4, 442628/2018-8, 442637/2018-7, respectively) and CMAR2 (CAPES grant number 23038.001421/2014-2030) projects. The authors thank to the crew of the RV Almirante Maximiano of the Brazilian Navy and several scientists and technicians participating in the cruise for their valuable help during sampling. We are grateful to Simon Wright, from the Australian Antarctic Division, for providing the CHEMTAX v.1.95 software and to Ricardo Pollery, from Federal University of Rio de Janeiro, for performing the nutrient analysis. T. Monteiro and T.S. Dotto acknowledge financial support from the CAPES Foundation and CNPq-Brazil PDJ scholarship (151248/2019-2), respectively. RR. Costa, C.R.B. Mendes, R. Kerr, C. Odebrecht and E.R. Secchi are granted with research fellowships from CNPq. CAPES also provided free access to many relevant journals though the portal "Periódicos CAPES." This study is within the scope of two Projects of the Institutional Internationalization Program (Capes PrInt-FURG–Edital 41/2017). We are thankful for the constructive criticism of two anonymous reviewers, which helped to improve the manuscript.

Conflict of Interest

All authors declare they have no conflict of interests.

Submitted 31 October 2019
Revised 03 February 2020
Accepted 15 February 2020

Associate editor: Heidi Sosik